Changes in Under-Ice Primary Production in the Chukchi Sea From 1988 to 2018

C. M. Payne[1] , L. Bianucci[2] , G. L. van Dijken[1] , and K. R. Arrigo[1]

[1]Department of Earth System Science, Stanford University, Stanford, CA, USA, [2]Institute of Ocean Sciences, Fisheries and Oceans, Sidney, BC, Canada

Abstract Changes in sea ice thickness and extent have corresponded with substantial changes in net primary production (NPP) in the Arctic Ocean. In recent years, observations of massive phytoplankton blooms under sea ice have upended the previous paradigm that Arctic NPP was driven largely by growth in the marginal ice zone and open water periods. Here, a new 1-D biogeochemical model capable of simulating ice algal and phytoplankton dynamics both under the ice and in open waters is applied in the northern Chukchi Sea for the years 1988–2018. Over this period, substantial under-ice (UI) blooms were produced in all but four years and were the primary drivers of interannual variation in total NPP. While NPP in the UI period was highly variable interannually due to fluctuations in ice thickness and the length of the UI period, UI NPP accounted for nearly half of total NPP between 1988 and 2018. Further, years with high UI NPP had reduced annual zooplankton grazing, indicating an intensification in the mismatch between phytoplankton and zooplankton populations and possibly altering the partitioning of food between benthic and pelagic ecosystems. These results demonstrate that the often-overlooked ice covered period can be highly productive in the Arctic Ocean, and that the northern Chukchi Sea has been amenable to UIB formation since at least 1988.

Plain Language Summary Historically, the ice-covered part of the year was not thought to contribute substantially to primary production in the Chukchi Sea sector of the western Arctic Ocean. However, observations of massive under-ice blooms suggest that, as ice has thinned due to climate change, an increase in under-ice light has allowed these phytoplankton to bloom earlier in the year. We built a model to investigate how changes in ice conditions in the Chukchi Sea have impacted phytoplankton production. We found that under-ice production accounted for nearly half of total productivity between 1988 and 2018, and that under-ice blooms could have formed as early as 1988 in the Chukchi Sea. Further, we found that zooplankton grazing was reduced in years with high under-ice production, indicating an intensification in the mismatch between phytoplankton and zooplankton. This could impact the food available to other organisms in the ecosystem and the amount of carbon that sinks to the sediments.

1. Introduction

As a result of the amplified effects of anthropogenic climate change in the polar regions (Screen & Simmonds, 2010), the Arctic is warming more rapidly than anywhere else in the world (Stocker et al., 2013). These rising temperatures have contributed to the changing sea ice conditions observed in the Arctic over the past several decades. Sea ice extent has diminished markedly and the rate of change is accelerating; between 1997 and 2014, sea ice coverage shrank at a rate four times greater than that between 1979 and 1996 (Serreze & Stroeve, 2015). Additionally, sea ice thickness has declined across the Arctic basin; between 2003 and 2012, the thickness of the sea ice pack decreased by an average of 7.5 cm yr^{-1} (Laxon et al., 2013). Part of this reduction in thickness is due to the loss of multi-year ice at a rate of 15%–17% per decade between 1979 and 2011 (Comiso, 2012). By 2014, only one quarter of the areal coverage of 5+ year-old sea ice observed in the 1980s remained (Serreze & Stroeve, 2015). Thinner and younger sea ice has also led to the proliferation of melt ponds on the surface of the ice (Webster et al., 2015) and substantially reduced Arctic albedo (Perovich & Polashenski, 2012).

Sea ice loss has already had large-scale impacts on Arctic Ocean ecosystems. As sea ice extent declined between 1998 and 2018, open water area increased by 27%, contributing to a 57% increase in net primary production (NPP) during the open water period (Lewis et al., 2020). As sea ice formation shifts later in the

year, wind-driven mixing has allowed fall blooms to form (Ardyna et al., 2014). There is even substantial evidence that the ice-covered part of the year, a period historically assumed to be too light-limited to allow for much phytoplankton productivity, can support massive under-ice blooms (UIBs). For instance, phytoplankton biomass exceeded 1291 mg chlorophyll *a* (Chl *a*) m^{-2} in a UIB observed in the Chukchi Sea in the western Arctic Ocean (Arrigo et al., 2012, 2014). While UIBs have been sporadically noted throughout the Arctic Ocean (Apollonio & Matrai, 2011; English, 1961; Fortier et al., 2002; Strass & Nöthig, 1996; Yager et al., 2001), observations of these blooms have become more frequent in recent years (Arrigo et al., 2012, 2014; Assmy et al., 2017; Boles et al., 2020; Hill, Light, et al., 2018; Leu et al., 2011; Mundy et al., 2009, 2014; Oziel et al., 2019; Randelhoff et al., 2020), perhaps suggesting that changing ice conditions may be more amenable to UIB formation. The thinner, melt pond-covered sea ice that now dominates much of the Arctic Ocean can transmit substantially more light into the underlying water column (Light et al., 2015; Webster et al., 2015). Horvat et al. (2017) found that, largely due to thinning sea ice, up to 30% of the Arctic Ocean had sufficient light to support a UIB between 2006 and 2015. Increasing under-ice light penetration may substantially increase the probability of UIB formation and thus the magnitude of carbon (C) fixed under the ice. These earlier blooms may further enhance the mismatch between phytoplankton and zooplankton populations in cold Arctic waters (Conover & Huntley, 1991).

Here we present a new 1-D nitrogen, phytoplankton, zooplankton, and detritus (NPZD) biogeochemical model, which we refer to as the Coupled Arctic Ocean System (CAOS) model. CAOS is coupled to an existing physical model (GOTM; Burchard et al., 1999) and a sedimentary chemistry model (OMEX-DIA; Soetaert et al., 1996b) to determine if changing atmospheric and sea ice conditions between 1988 and 2018 have altered annual NPP in the northern Chukchi Sea where the massive UIB was observed (Arrigo et al., 2012, 2014). In this study, we assess the relative magnitude of NPP during the under-ice, marginal ice zone, and open water periods from 1988 to 2018 and evaluate which environmental variables are the most important in controlling the magnitude of under-ice NPP.

2. Methods

2.1. Study Site

The three coupled 1-D models (Figure 1), CAOS-GO, were forced with both satellite-derived and reanalysis data for 72.16°N and 166.60°W (Figure 2). This location is in the midst of the massive phytoplankton bloom observed on the Chukchi shelf in 2011 (Arrigo et al., 2014). It is located along a major flowpath of Anadyr and Bering Shelf water advected through the Bering Strait and is 107 km from the shelf break (Figure 2; shelf break = 200 m isobath), so the influence of physical processes associated with the shelf break is likely to be minimal.

2.2. Physical Model

The 1-D General Ocean Turbulence Model (GOTM, version 5.4; Burchard et al., 1999) was used to generate temperature, salinity, buoyancy frequency, and turbulent diffusion coefficient timeseries. GOTM was run with a water column composed of 50 vertical layers of 1 m thickness and timesteps of 1 h.

GOTM does not directly include a dynamic ice model. To account for the effects of sea ice cover on heat flux, GOTM was modified such that when satellite-derived sea ice concentration surpassed 90% (see Section 2.5), the heat flux across the air-sea boundary was set to zero and surface water temperatures remained at the salinity-dependent freezing point of seawater (where the freezing point of water in °C is −0.0575 times the salinity, or −1.90°C at the wintertime surface salinity). The effect of sea ice cover on wind momentum flux to the surface ocean was simulated as described by Schulze and Pickart (2012), who found that wind momentum was transmitted through fully consolidated pack ice at a reduced rate when compared to open-water conditions, but that partial coverage resulted in an increase in wind momentum flux. As a result, when sea ice concentration is ≥90%, the model transmits 76% of wind momentum to the ocean; at sea ice concentrations of >10% and <90%, the model transmits 126% of the momentum to the ocean; and when sea ice concentration is ≤10%, 100% of the momentum is transmitted to the ocean (Schulze & Pickart, 2012). See Section 2.5 for details on the sea ice concentration input.
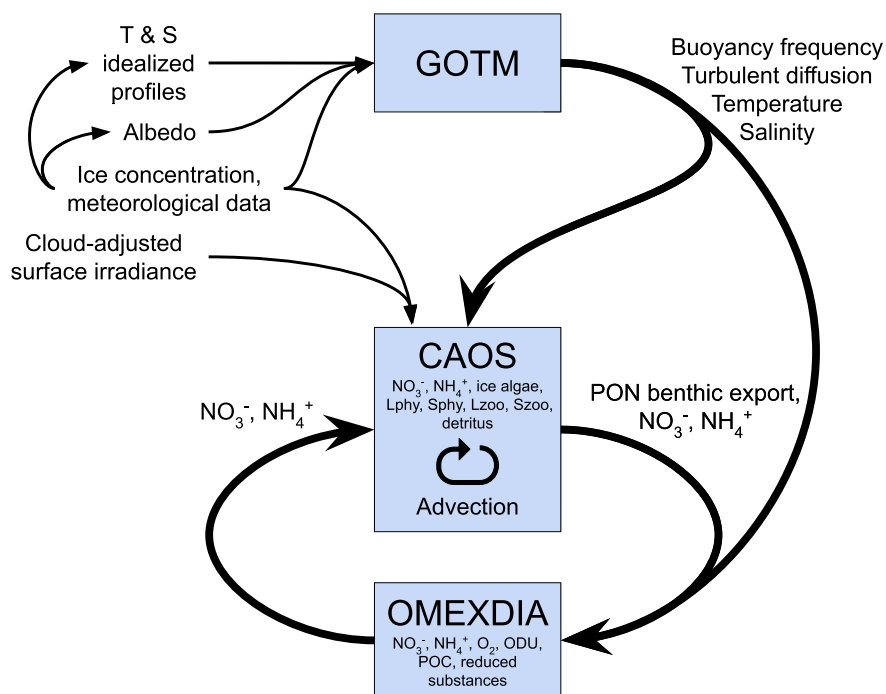
Figure 1. An overview of the inputs and outputs shared between the 3 models (GOTM, CAOS, and OMEXDIA) in CAOS-GO. Thick lines represent flows between models, while thin lines represent external inputs to the models. State variables are listed in small text for the CAOS and OMEXDIA models.

GOTM was further modified to reflect the effects of surface type (ice, snow, or melt pond) on albedo and thus shortwave radiative heating of the surface ocean. Different albedo time series were used for each year of the model run to simulate changes in snow, ice, and melt pond conditions. Albedo for different surface types and rates of change of albedo in the Chukchi Sea (Figure S1) were adapted from Perovich and Polashenski (2012), while timings matched those of the prescribed ice conditions, described in Section 2.5. See Text S1.1 for more details on modifications to albedxso.

To compensate for processes not included in our modified version of GOTM (including horizontal advection, precipitation, and sea ice melt), modeled temperature and salinity were relaxed toward idealized profiles (see Text S1.2) on a timescale of 5 days for salinity and 15 days for temperature. Idealized temperature and salinity profiles (Figure S2) were created using remote sensing products and cruise data from 2011 and 2014 (Pacini et al., 2019). The mixed layer temperature of the idealized profiles was set using satellite-derived sea surface temperature (SST) when not ice-covered. CTD data collected at ICESCAPE 2011 stations (4-5 July and 8 July, 2011) and SUBICE stations (16 May to 20 June 2014) were used to determine the mixed layer depth and the thickness of the thermocline. To reflect annual differences in freshwater input to the water column, the salinity in the mixed layer for each year's idealized profiles was scaled from the 2011 profiles depending on the length of the sea ice melt period. Although increasing river runoff and meltwater has altered the salinity of the Arctic Ocean (Mauritzen, 2012; Woodgate et al., 2005, 2012), our model does not account for these changes. See Text S1.2 for more details on idealized profiles.

2.3. Biogeochemical Model

The CAOS model is a modified version of a nitrogen (N) based biogeochemical model for the Ross Sea, Antarctica (Arrigo et al., 2003). CAOS uses GOTM-derived temperature, buoyancy frequency (for determining mixed layer depth), and turbulent diffusion (which is added to a background turbulent diffusivity of 5×10^{-4} m^2 s^{-1} - Rainville & Winsor, 2008) as physical inputs (see Section 2.2). Surface spectral irradiance is determined using the radiative transfer model of Gregg and Carder (1990), adjusted for cloud cover (Dobson & Smith, 1988). CAOS then computes transmission of spectral photosynthetically available
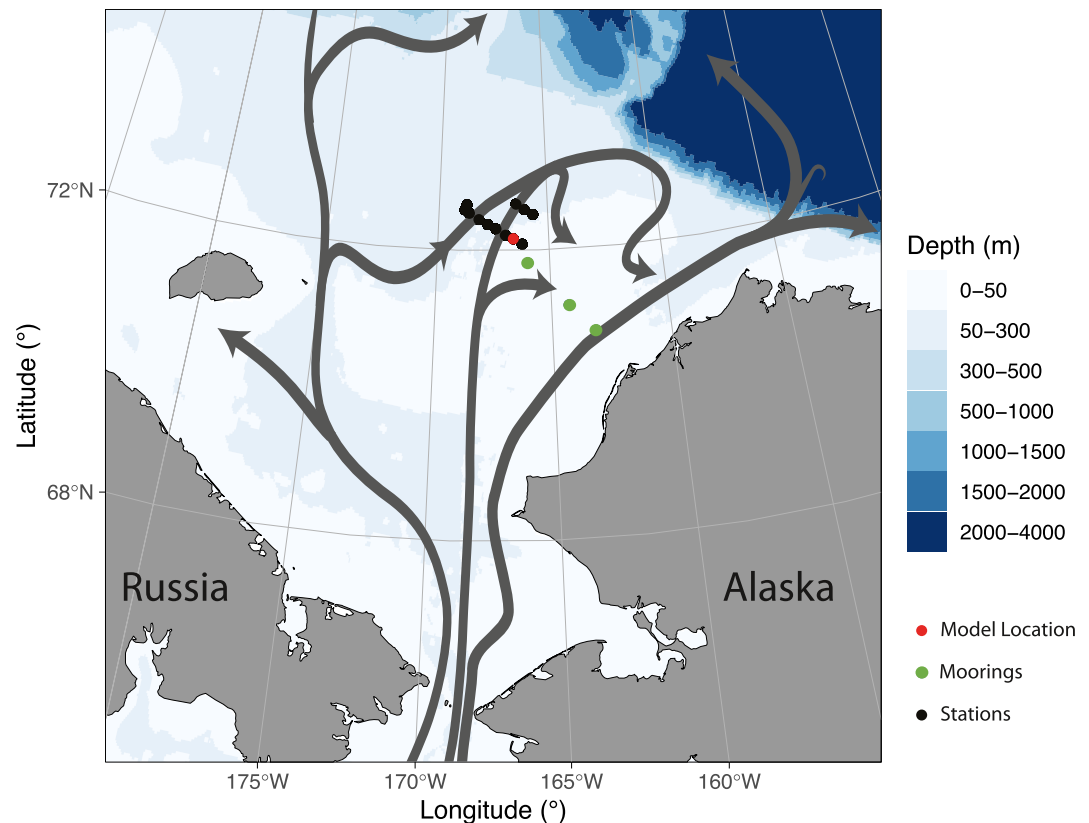
Figure 2. Bathymetric map of the Chukchi Sea including schematic flow paths of advected water (gray lines, after Corlett & Pickart, 2017). Points represent the location of the model (red), ICESCAPE 2011 stations used to create idealized profiles (black), and moorings used to evaluate model performance (green; Mordy et al., 2020).

and usable radiation (PAR and PUR, respectively) through the sea ice and into the water column (Arrigo et al., 1991, 1998; Morel, 1978; Perovich et al., 1986) using seasonally variable absorption coefficients (Bricaud et al., 1995; Lewis & Arrigo, 2020) according to Beer's law (see Text S2.1 for radiative transfer equations).

CAOS dynamically models ice algae, large and small phytoplankton, large and small zooplankton (Ashjian et al., 2003; B. F. Sherr et al., 2008; E. B. Sherr et al., 2009), detritus, and two inorganic N pools, nitrate (NO_3^-) and ammonium (NH_4^+; Figure 3). The model calculates PON export to the benthos, which is used as input for the sediment model OMEXDIA (see Section 2.4). The CAOS model is run with a 15 min timestep. See Text S2.2–S2.7 for all model equations.

In order to run the model for multiple years in the Chukchi Sea, which is characterized by the northward advection of NO_3^--replete waters through the Bering Strait, horizontal advection must be included. The effects of advection are simulated by relaxing all state variables toward prescribed profiles. Often, this is done by using observational data. However, there are not sufficiently high-quality observational data to provide prescribed profiles of all state variables between 1988 and 2018. Instead, we took advantage of the fact that water advects from the south in the Chukchi Sea; sea ice cover of this advecting water diminishes earlier, allowing an earlier start to phytoplankton growth. This was accomplished by running the model twice; model profiles generated for Day+1 (first run) were used as prescribed profiles for Day+0 (second run). NO_3^- profiles were further modified following day of year (DOY) 300 so that NO_3^- concentrations were gradually restored to 16 mmol m^{-3} throughout the water column (see Text S2.7). In the first run only, state variables were reset to the initial conditions on January 1 each year. While this relaxation was necessary to approximate the typical seasonal cycle of NO_3^-, the strength of the relaxation and length of time of the offset were chosen to minimize impacts on other state variables. For example, large phytoplankton blooms simulated with and without advection were statistically comparable (slope = 1.0023, R^2 = 0.997, $p<0.001$).
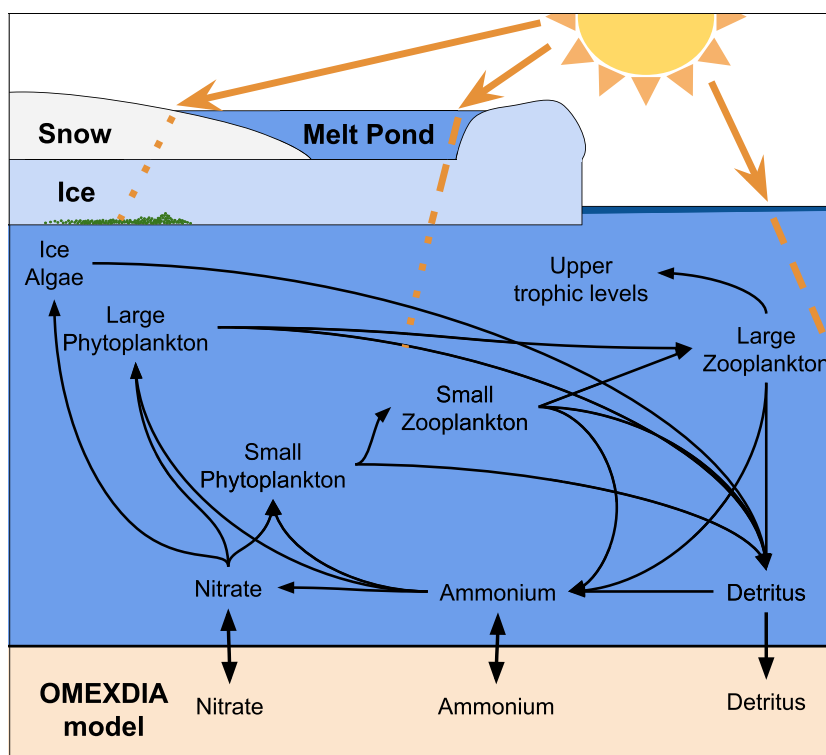
Figure 3. A diagram of the CAOS model. Light passes through snow, ice, and/or melt ponds depending on ice conditions. Black arrows represent N exchange between state variables (text). Upper trophic levels are not explicitly modeled, but mortality of zooplankton is assumed to contribute to upper trophic levels. Detritus that is exported to the benthos and the bottom layer concentrations of two inorganic nitrogen state variables (nitrate and ammonium) are also used as input for the sediment model, OMEXDIA.

2.4. Sediment Model

The sedimentary component of our model is OMEXDIA, the early diagenetic model by Soetaert et al. (1996b), implemented dynamically in *R* using the ReacTran (Soetaert & Meysman, 2012) and deSolve (Soetaert et al., 2010) packages. OMEXDIA simulates daily changes in fast- and slow-remineralizing organic matter classes, oxygen (O_2), NO_3^-, NH_4^+, and a reduced substances state variable. The model calculates rates of oxic and anoxic mineralization, nitrification, denitrification, and the production of solid inorganic C-containing minerals in ocean sediments. For full details of the OMEXDIA model equations, see Soetaert et al. (1996b).

OMEXDIA was run with a time step of one day over the top 0.5 m of the sediments, with 100 layers of a thickness increasing exponentially from 0.1 mm at the surface to 20 mm at the deepest layer (according to $y = 0.094e^{0.568x}$, where y is the layer thickness and x is the layer number). The model uses as input daily mean bottom water salinity and temperature from GOTM, as well as daily mean bottom water NO_3^- and NH_4^+ concentrations and a daily summed PON benthic export (converted to C export) from CAOS.

2.5. Model Forcing

Meteorological conditions (wind, air temperature, pressure, relative humidity, and cloud cover) were set using the National Centers for Environmental Prediction (NCEP) North American Regional Reanalysis (NARR; 32 km resolution used in this model configuration) products, provided by the NOAA/OAR/ESRL PSL, Boulder, Colorado, USA from their website at: https://psl.noaa.gov/data/gridded/. Additionally, as mentioned in Section 2.2, GOTM temperatures were nudged toward idealized profiles, with temperatures over the mixed layer set using NOAA OISST version 2.1 (0.25° latitude and longitude resolution; Reynolds et al., 2007) data, provided by the NOAA/OAR/ESRL PSL, Boulder, Colorado, USA, from their website at https://psl.noaa.gov/.

Table 1
CAOS Model State Variables and Initial Values

State Variable	Description	Initial value
IA	Ice algae	0.0
Sphy	Small phytoplankton functional group	0.05 [a]
Lphy	Large phytoplankton functional group	0.05 [a]
Szoo	Small zooplankton functional group	0.01 [a]
Lzoo	Small phytoplankton functional group	0.01 [a]
Detri	Detritus functional group	0.0
NO_3^-	Dissolved nitrate concentration	16.0
NH_4^+	Dissolved ammonium concentration	0.0

Note. All are in units of mmol N m^{-3}.

[a]indicates that the initial value is also a minimum value.

Snow and melt pond thickness were computed using the mean of two Arctic Ocean snow depth models, SnowModel-LG (Liston et al., 2020; Stroeve et al., 2020, 25 km resolution, ERA5 forcing) and CPOM (Zhou et al., 2021, 12.5 km resolution, ERA-Interim forcing). Sea ice thickness was derived from ice age (Tschudi et al., 2019, 62.5 km resolution, ERA-Interim forcing) by fitting a compilation of average February–March (2004–2008) ice thickness by age (Tschudi et al., 2016). Melt pond areal coverage was also estimated based on satellite-derived ice age (Tschudi et al., 2019), with a more rapid increase and higher maximum in melt pond areal coverage for first-year sea ice (1.39% d^{-1}, up to 54% areal coverage) than for multi-year ice (0.64% d^{-1}, up to 38% areal coverage), as in Webster et al. (2015). See Text S3.1–S3.3 for more details on deriving ice, snow, and melt pond layer thicknesses and melt pond areal coverage from satellite observations.

The onset of snow melt was set using the mean National Snow and Ice Data Center (NSIDC) snow melt onset date (Anderson et al., 2019, 75 km resolution; see Text S3.4 for more details on the snow melt date). Sea ice began to melt (and melt ponds began to form) on the first 24-h period when the mean NCEP NARR 2 m air temperature exceeded 0°C at the model location. Following the ice melt date, melt pond thickness increased to its maximal thickness (90% of the maximum snow thickness) by the start of sea ice retreat. Over this same period, sea ice thickness decreased by 0.0073 m d^{-1}, or 50% of the total ice melt necessary to produce the idealized salinity profiles. For the duration of sea ice retreat, sea ice and melt pond thickness remained fixed. The timing of the start and end of sea ice retreat and advance were set based on the sea ice concentration (75 km resolution), provided by the NOAA/NSIDC Climate Data Record sea ice concentration (Meier et al., 2019; Peng et al., 2013). Sea ice retreat starts when satellite-derived ice cover diminished below 90% and ends when ice concentration decreased below 10%. Between these dates, sea ice extent diminishes linearly. Following ice retreat, open water persisted until the start of ice advance, the date at which satellite-derived ice concentration increased above 10%. Sea ice concentration then increased linearly until the date when satellite-derived concentration surpassed 90%.

2.6. Initialization and Parameterization

The models are spun up for one year using the same input data for the first two years before proceeding to subsequent years; the first year is excluded from further analysis. State variables for each model run are initialized with identical concentrations in all layers of the water column (Table 1). For both phytoplankton and zooplankton size classes, these initial values are also minimum values, and state variables are not allowed to diminish below these values.

GOTM parameters used in the standard run matched those used in the OWS Papa test case (https://gotm.net/cases/ows_papa/), with the exception of those used to control meteorological fluxes, which were calculated using the formulation of Kondo (1975). For a full list of GOTM model equations and parameters, see Burchard et al. (1999). Parameters for the standard run of CAOS are listed in Table 2. Parameters for the standard run of OMEXDIA that differ from those used in Soetaert et al. (1996b) are listed in Table 3. For a full list of OMEXDIA model parameters, see Soetaert et al. (1996a). and Soetaert et al. (1996b). For a description of methods used to evaluate model performance, including comparing modeled and satellite NPP (Arrigo et al., 2008; Lewis & Arrigo, 2020; Pabi et al., 2008) and modeled and observed NO_3^- (Arrigo et al., 2017; Lowry et al., 2015; Mordy et al., 2020) and sensitivity analysis, see Sections S4.1 and S4.2. For a description of the evaluation of model performance and sensitivity analysis, see Sections S5.1–S5.3.

2.7. Primary Production

Ice algal (IA) NPP was computed from the daily change in modeled ice algal Chl *a* concentration, using an algal C:Chl ratio of 35 (Cota & Home, 1989, see Text S2.2 for ice algal equations). IA NPP extended from bloom initiation (when light reached the compensation irradiance, 2.0 μmol photons m^{-2} s^{-1}, in the bottom

Table 2
CAOS Model Parameters: Parameter Descriptions, Values, Units, and Sources of Parameters Used

Parameter	Description	Value	Unit	Source
IA_L	Maximum ice algal Chl *a* concentration	30	mg Chl *a* m^{-2}	a
IA_{x0}	Sigmoid midpoint for logistical curve describing ice algal growth	14	D	b
IA_k	Ice algal logistical growth rate	0.4	mg Chl *a* m^{-2} d^{-1}	b
$IA_{comp.irrad.}$	Compensation irradiance for ice algae	2.0	μmol photons m^{-2} s^{-1}	c
$loss_{IA}$	Disassociation rate of ice algae	0.05	d^{-1}	d
E_{k_Lphy}	Observed photoacclimation parameter, E_k, for large phytoplankton	54.9–67.6	μmol photons m^{-2} s^{-1}	e, *
μ_{0_Lphy}	Specific growth rate for large phytoplankton at 0°C	1.78	d^{-1}	e, **
$mort_{Lphy}$	Death and loss rate of large phytoplankton	0.065	d^{-1}	d
$K_{s\_NO3\_Lphy}$	Half-saturation constant for NO_3^- uptake by large phytoplankton	0.9	mmol N m^{-3}	-
$K_{s\_NH4\_Lphy}$	Half-saturation constant for NH_4^+ uptake by large phytoplankton	0.7	mmol N m^{-3}	-
C/N_{Lphy}	Carbon to nitrogen ratio of large phytoplankton	106/14	mol:mol	f, g
C/Chl_{Lphy}	Carbon to Chl *a* ratio of large phytoplankton	60	g:g	g
E_{k_Sphy}	Observed photoacclimation parameter, E_k, for small phytoplankton	100	μmol photons m^{-2} s^{-1}	h, *
μ_{0_Sphy}	Specific growth rate for small phytoplankton at 0°C	1	d^{-1}	e, **
$mort_{Sphy}$	Death and loss rate of small phytoplankton	0.045	d^{-1}	d
$K_{s\_NO3\_Sphy}$	Half-saturation constant for NO_3^- uptake by small phytoplankton	0.3	d^{-1}	-
$K_{s\_NH4\_Sphy}$	Half-saturation constant for NH_4^+ uptake by small phytoplankton	0.1	mmol N m^{-3}	-
C/N_{Sphy}	Carbon to nitrogen ratio of small phytoplankton	106/16	mol:mol	i
C/Chl_{Sphy}	Carbon to Chl *a* ratio of small phytoplankton	100	g:g	j
$Sphy_{scarce}$	Sphy scarcity threshold: Szoo consumption is adjusted by Sphy/$Sphy_{scarce}$	0.5	mmol N m	-
$mort_{zoo}$	Zooplankton mortality rate	0.05	d^{-1}	d
ex_{zoo}	Zooplankton excretion rate	0.1	d^{-1}	d
γ	Zooplankton unassimilated grazing fraction	0.25	d^{-1}	d
$K_{s\_Sphy\_Szoo}$	Half-saturation constant for small phytoplankton uptake by small zooplankton	0.5	mmol N m^{-3}	-
$K_{s\_Lphy\_Lzoo}$	Half-saturation constant for large phytoplankton uptake by large zooplankton	0.5	mmol N m^{-3}	-
$K_{s\_Szoo\_Lzoo}$	Half-saturation constant for small zooplankton uptake by large zooplankton	0.5	mmol N m^{-3}	-
$Remin_{Det \to NH4}$	Remineralization rate of detritus to NH_4^+	0.2	mmol N m^{-3}	k
w_{det}	Detrital sinking rate	5	m d^{-1}	b
C/N_{det}	Carbon to nitrogen ratio of detritus	106/15.8	mol:mol	j
$Nitr\_m_{NH4 \to NO3}$	Slope for the depth-dependent nitrification rate	0.5824	mmol N m^{-4}	l
$Nitr\_b_{NH4 \to NO3}$	*Y*-intercept for the depth-dependent nitrification rate (values below 0 = 0)	−3.4313	mmol N m^{-3}	l

Note. * Reported E_k values were measured for PAR. Since phytoplankton functional groups were modeled using PUR, these values were modified in the model to reflect that only 38.3% of photosynthetron-produced light is usable by phytoplankton. ** Reported growth rates of 0.89 and 1.6 days^{-1} were observed at −1.6°C. These values were adjusted using the Eppley (1972) temperature/growth relationship to calculate specific growth rates at 0°C
[a]Arrigo (2017). [b]Welch and Bergmann (1989). [c]McMinn et al. (1999). [d]Arrigo et al. (2014). [e]Fasham et al. (1990). [f]Brzezinski (1985); Lomas et al. (2019). [g]ICESCAPE 2011 data. [h]Lewis et al. (2019). [i]Redfield (1958). [j]Sakshaug (2004). [k]Davis and Benner (2007). [l]SUBICE 2014 data.

layer of the ice) until the start of ice melt and meltpond formation, and was integrated annually. Daily phytoplankton NPP was integrated with respect to depth over three different time periods based on sea ice conditions. The under-ice (UI) period extended from the initiation of phytoplankton growth (the date when daily phytoplankton NPP increases above 0.05 g C m^{-2} d^{-1}) until the start of sea ice retreat. The marginal ice

Table 3
Parameters Used in the OMEXDIA Model That Differ From Those in Soetaert et al. (1996b)

Parameter	Description	Value	Unit	Source
F_{fast}	Flux of fast-decaying detritus	(*)	g C m^{-2} yr^{-1}	a
F_{slow}	Flux of slow-decaying detritus	(*)	g C m^{-2} yr^{-1}	a
p_{fast}	Proportion of fast-decaying detritus	0.5	d^{-1}	b
R_{fast}	Decay rate for the fast-decaying detritus	0.18	d^{-1}	c
R_{slow}	Decay rate for the slow-decaying detritus	0.005	d^{-1}	b
$k_{in}(O_2$ denit)	Half saturation conc. for O_2 inhibition in denitrification	15	mmol O_2 m^{-3}	d
$k_{in}(NO_3^-$ anox)	Half saturation conc. for NO_3^- inhibition in anoxic mineralization	1	mmol NO_3^- m^{-3}	d
$k_{in}(O_2$ anox)	Half saturation conc. for O_2 inhibition in anoxic mineralization	1	mmol NO_3^- m^{-3}	d
C/N_{fast}	Carbon to nitrogen ratio of fast-decaying detritus	106/14.18	mol:mol	a
C/N_{slow}	Carbon to nitrogen ratio of slow-decaying detritus	106/12.1	mol:mol	e
ϕ_0	Porosity at the sediment-water interface	0.915	-	d
coeffϕ	Coefficient for exponential porosity changes	4	-	b
Db_0	Constant bioturbation coefficient in the bioturbated layer	2	cm^2 yr^{-1}	f
x_b	Depth below which bioturbation decays exponentially	3	Cm	f
O_2_bw	Oxygen concentration of the bottom water NO_3^-	300	mmol N m^{-3}	**
$NO_3^-\_bw$	Daily mean bottom-water NO_3^-	(*)	mmol N m^{-3}	a
$NH_4^+\_bw$	Daily mean bottom-water NH_4^+	(*)	mmol N m^{-3}	a
W	Sedimentation rate	0.35	cm y^{-1}	e, g
Temperature	Daily mean bottom-water temperature	(*)	°C	a
Salinity	Daily mean bottom-water salinity	(*)	-	a

Note. (*) Variable conditions produced by GOTM or the CAOS model. ** Mean oxygen concentration for the stations closest to the model location for ICESCAPE 2011.
[a]from CAOS model. [b]Soetaert et al. (1996b). [c]Davis and Benner (2007). [d]Soetaert et al. (1996a). [e]Cooper and Grebmeier (2018). [f]Teal et al. (2008). [g]Darby et al. (2009).

zone (MIZ) period extended from the start until the end of ice retreat. Finally, the open water (OW) period was initiated at the end of ice retreat. The OW period ended on the earliest date when light was reduced in the water column: either when sea ice advanced in the autumn, or when light diminished below 1% the maximum value reached in the mixed layer (DOY 300 ± 6). NPP was also integrated both daily and monthly, and zooplankton grazing of both phytoplankton classes was integrated monthly, annually, and within the UI, MIZ, and OW periods.

NPP was further divided into new, regenerated, surface, and subsurface production. All NO_3^--based NPP was considered new production, while NH_4^+-based NPP was considered regenerated production. To determine if production was located in the surface or subsurface, for each day of the model run, large phytoplankton biomass for each layer (z) of the water column below 10 m was compared to the layer above (z-1). If the lower layer (z) had >110% of the biomass in the layer above (z-1), that layer was considered to be the upper boundary of the subsurface Chl *a* maximum (SCM). Total NPP above that depth was then defined as surface NPP, while NPP at or below that depth was defined as NPP within the SCM. If no obvious SCM existed (z was always < 110% of z-1), water column NPP was integrated and was considered to be surface NPP.

2.8. Statistics

Multiple linear regression was used to assess the relative importance of ice and snow layer thicknesses and changing ice condition dates in controlling NPP. Ice variables were assessed for collinearity using the variance inflation factor (VIF). VIF was <3 for all ice variables, indicating only moderate correlation among layer thickness and ice condition date variables. The multiple linear regression that best fit data was identified

using backward selection by sequentially eliminating the variable with the highest p-value until only statistically significant variables ($p<0.05$) remained. Regressions were visually inspected to ensure that the relationships between independent and dependent variables were linear. Regressions were also checked to ensure that the residuals were normally distributed using the Shapiro-Wilk test and thorough visual inspection of histograms and Quantile-Quantile plots. The relative importance of each variable in the multiple linear regression model was calculated using the "relaimpo" package in *R*.

Annual cycles of daily NPP were clustered using k-means clustering based on NPP in the UI and MIZ periods. The optimal *k* value was determined using the gap statistic. ANOVA and post hoc Tukey's honest significant difference (HSD) tests were then used on the clusters to assess the relationship between ice conditions and annual cycle type. All statistical analysis was conducted in *R*.

3. Results

In most years (such as the standard run year, 2011; Figure 4), sea ice algae begin to grow at the bottom of the ice in the spring and draw down NO_3^- from surface waters. As air temperatures increase and sea ice and snow begin to melt, the ice algal bloom sloughs off the bottom of the ice and sinks through the water column to the sea floor. The remineralization of this organic matter allows NH_4^+ to accumulate in surface waters (in concentrations of 0.45 ± 0.32 mmol m^{-3}; Figure 4b), where little NH_4^+ is nitrified. Soon thereafter, the biomass of large phytoplankton in the mixed layer increases rapidly beneath the sea ice as light in the water column increases, reaching an average maximum of 24.9 ± 3.3 mg Chl *a* m (Figure 4c). This phytoplankton bloom rapidly takes up NO_3^- and NH_4^+ over the upper 30 m (Figures 4a and 4b). Concentrations of large phytoplankton in the upper water column start to diminish around the time of sea ice retreat as NO_3^- is depleted. At the same time, NH_4^+ accumulates below the mixed layer (0.63 ± 0.20 mmol m^{-3}; Figure 4b) as detritus is remineralized, and nitrification in the water column and sediments allows bottom-water concentrations of NO_3^- to reach an autumn maximum of 32.4 ± 1.9 mmol m^{-3}.

During the OW period in the summer and fall, large phytoplankton biomass accumulates below the mixed layer where NO_3^- is still available, reaching mean concentrations of 11.5 ± 0.9 mg Chl *a* m^{-3}. Small phytoplankton also accumulate near the base of the mixed layer in the late summer and fall, but at concentrations of only 0.2 ± 0.1 mg Chl *a* m^{-3} (Figure 4d). Concentrations of large and small zooplankton rapidly increase once water column temperatures exceed 0°C and reach peak concentrations (of 0.05 ± 0.02 and 0.02 ± 0.01 mmol N m^{-3}, Figures 4e and 4f, for large and small zooplankton, respectively) in the late summer. These increases occur after large phytoplankton have descended to the SCM. As ice advances in the autumn, mean NO_3^- concentrations are slowly restored to the winter concentration of 16.2 ± 0.2 mmol m^{-3}.

3.1. Interannual Changes in Ice Conditions

Several satellite-derived snow and ice conditions changed significantly between 1988 and 2018 at the model location in the Chukchi Sea, while others showed no trend with time. The snow melt date advanced by 12.4 days per decade over this period ($R^2 = 0.139$, $p = 0.039$; Figure 5d). The start and end dates of sea ice retreat were earlier by 8.8 ($R^2 = 0.327$, $p<0.001$; Figure 5f) and 9.3 ($R^2 = 0.267$, $p = 0.003$; Figure 5g) days per decade, respectively. The date of ice advance, on the other hand, was delayed by 12.1 days per decade ($R^2 = 0.265$, $p = 0.004$; Figure 5h). Snow thickness diminished by 2.4 cm per decade ($R^2 = 0.206$, $p = 0.010$; Figure 5c). The sea ice melt date (when melt ponds formed and ice thickness began to diminish; Figure 5e) showed no statistically significant trend with time. Likewise, mean spring ice age (between March 1 and the start of ice retreat–see Text S1; Figure 5a) and age-derived thickness (Figure 5b) also showed no trend with time.

3.2. Interannual Changes in Total Annual NPP

Between 1988 and 2018, total (ice algal + phytoplankton) annual NPP ranged from 74.7 to 100.1 g C m^{-2} yr^{-1}, increasing annually by 0.34 g C m^{-2} yr^{-1} ($R^2 = 0.148$, $p = 0.033$; Figure 6a). New production ranged from 59.7 to 76.6 g C m^{-2} yr^{-1} (mean = 68.2 ± 4.7 g C m^{-2} yr^{-1}), with higher total annual NPP associated with
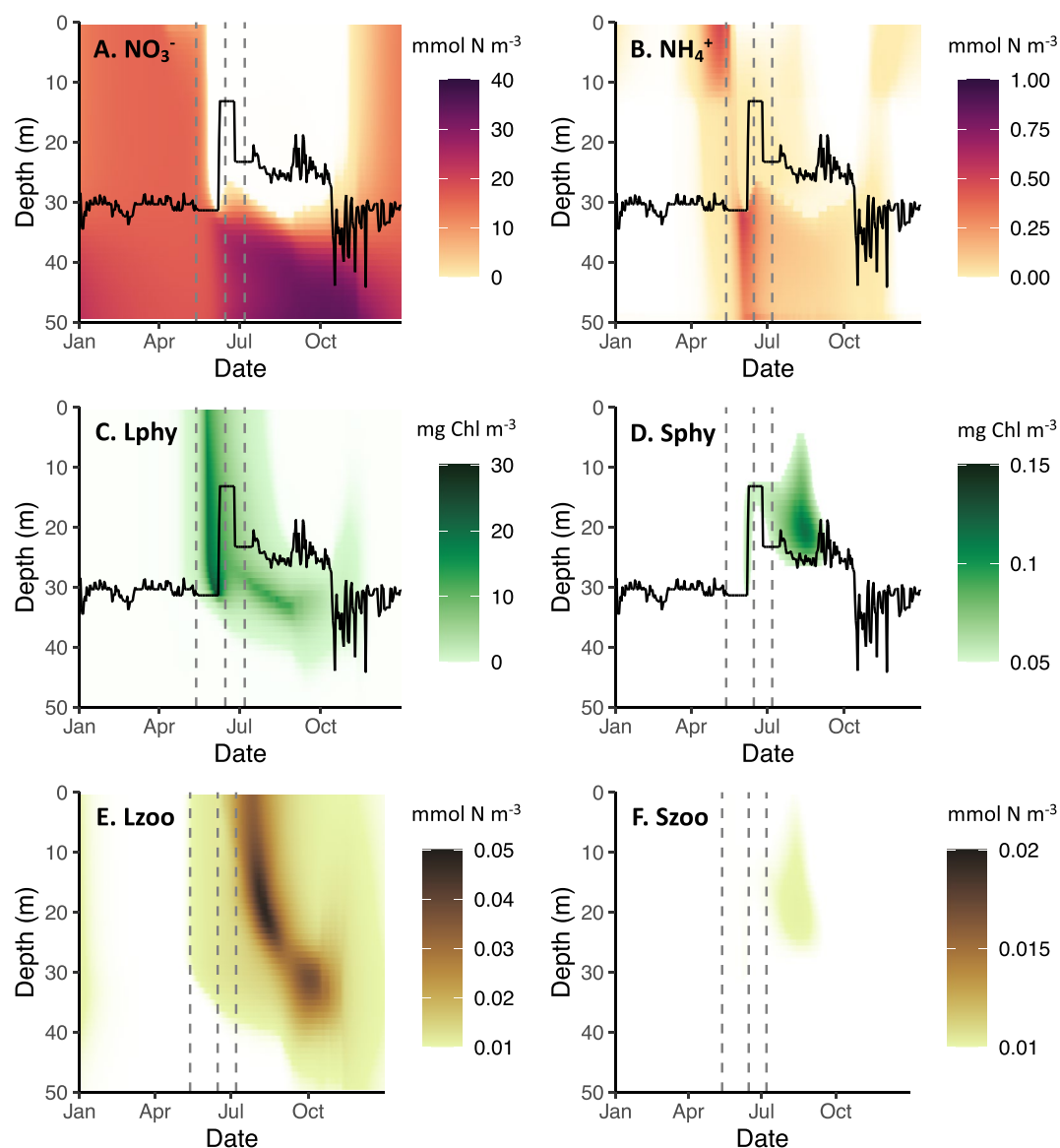
Figure 4. Annual depth versus time plots of (a) nitrate (NO_3^-), (b) ammonium (NH_4^+), (c) large phytoplankton (Lphy), (d) small phytoplankton (Sphy), (e) large zooplankton (Lzoo), and (f) small zooplankton (Szoo) for 2011, the standard run year. Black lines (a–d) represent the mixed layer depth, calculated based on GOTM-derived buoyancy frequency. Gray dashed lines on each subplot represent, from left to right, the date of ice melt, the start of ice retreat (which marks the end of the under-ice period and start of the marginal ice zone period), and the end of ice retreat (marking the end of the marginal ice zone period and beginning of the open water period).

higher new production ($R^2 = 0.852$, $p<0.001$). Multiple linear regression revealed that 75.2% of the variance ($p<0.001$) in total annual NPP is controlled by a combination of sea ice thickness ($R^2 = 0.387$, $p = 0.001$), the length of the UI period ($R^2 = 0.218$, $p = 0.031$), and the length of the OW period ($R^2 = 0.148$, $p = 0.002$).

3.3. Contributions by Ice Algae, UI, MIZ, and OW NPP to Total NPP

To assess the relative contribution by ice algae and phytoplankton to annual NPP, we divided the annual cycle into four periods: the ice algal (IA), the under-ice (UI), the marginal ice zone (MIZ), and the open water (OW) periods (see Section 2.7). Between 1988 and 2018, the IA period varied in length from 0 to 76 days, beginning between DOY 69 and 157 and ending between DOY 120 and 161. The length of the IA period increased by 1.1 d yr^{-1} ($R^2 = 0.168$, $p = 0.024$), driven by changes in the start of the IA period, which became
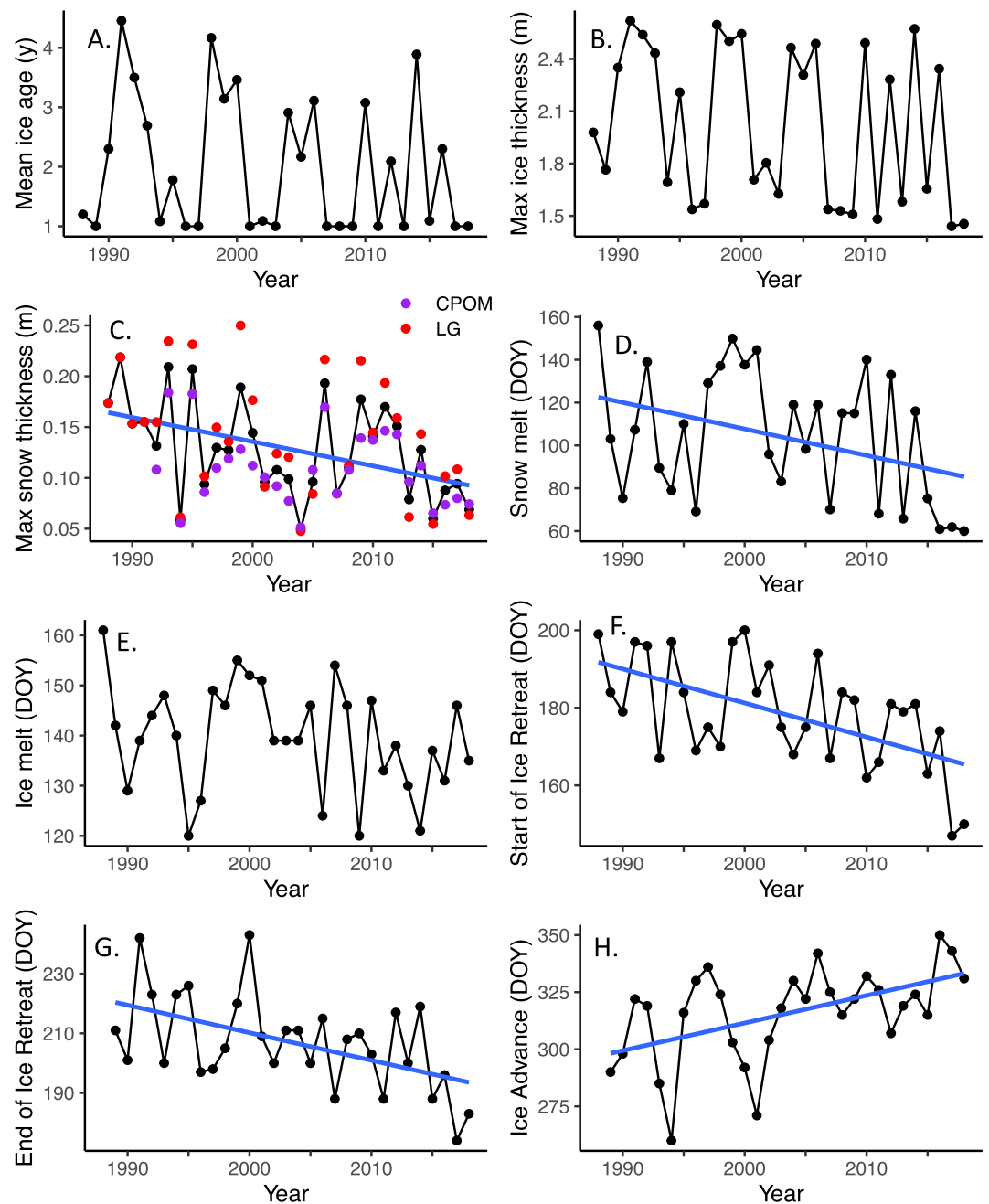
Figure 5. Ice and snow conditions between 1988 and 2018: (a) mean ice age (y), (b) maximum ice thickness (m), (c) maximum snow thickness (m), (d) snow melt date (day of year (DOY)), (e) ice melt date (DOY), (f) the date when ice retreat starts (DOY), (g) the date when ice retreat ends (DOY), and (h) the date when ice advances (DOY). Blue lines are used when linear regressions are statistically significant. For snow thickness, the mean (black) of two models, CPOM (purple) and SnowModel-LG (red), is used.

earlier by 1.4 days yr^{-1} ($R^2 = 0.224$, $p = 0.008$). The UI period varied in length from 6 to 91 days with no significant trend between 1988 and 2018. The UI period began between DOY 101 and 170 (mean = 137±21). Both the start and end of the UI period shifted earlier, by 1.1 d yr^{-1} ($R^2 = 0.238$, $p = 0.005$) and 0.9 days yr^{-1} ($R^2 = 0.327$, $p<0.001$), respectively. The MIZ period varied in length from 9 to 45 days over the study period, with the exception of 1988 when period length was 98 days because sea ice never fully retreated. There was no significant interannual change in MIZ period between 1988 and 2018. The OW period varied in length 50–128 days between 1989 and 2018 but was 0 days long in the anomalous sea ice year 1988. Between 1988
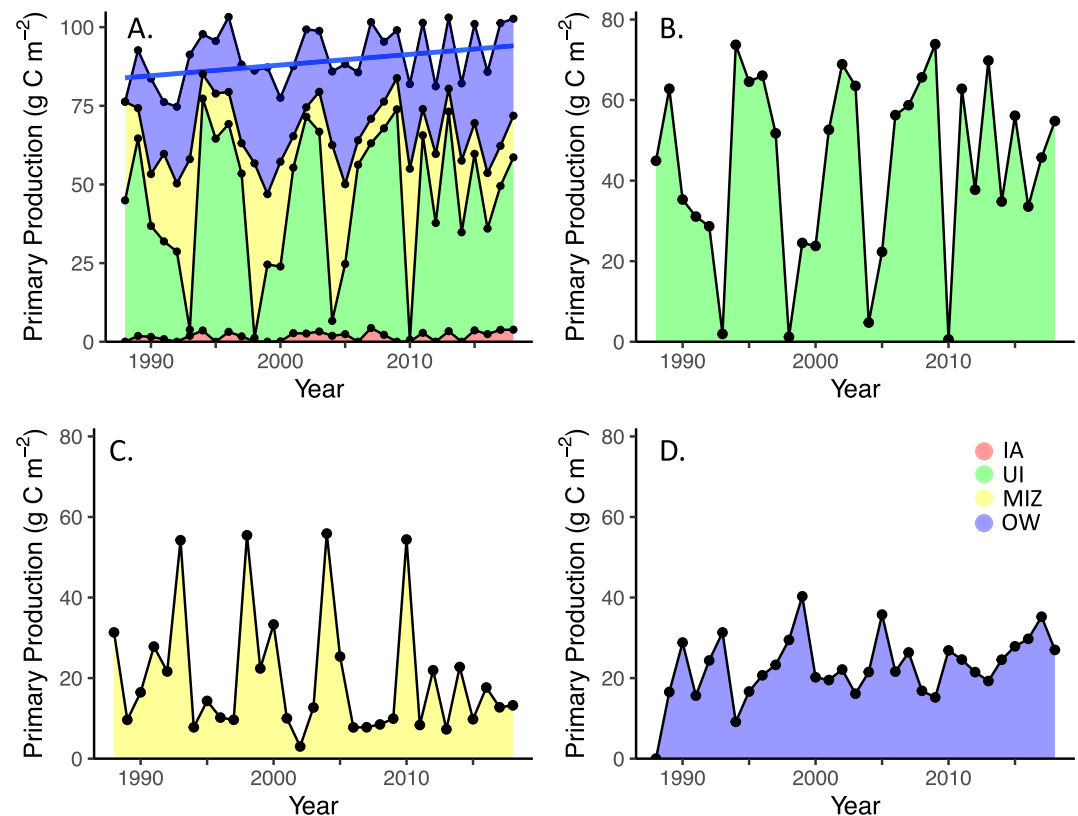
Figure 6. (a) Total annual net primary production (NPP; upper black line) and its component parts, (b) annual under-ice (UI) NPP, (c) annual marginal ice zone (MIZ) NPP, and (d) annual open water (OW) NPP between 1988 and 2018. Total annual NPP is composed of ice algal (IA) NPP (red), UI NPP (green), MIZ NPP (yellow), and OW NPP (blue). A blue line is used to indicate the statistically significant increase in total annual NPP.

and 2018, the length of the OW period increased by 15.1 days per decade ($R^2 = 0.309$, $p<0.001$) due to both earlier ice retreat and later ice advance.

Annual sea ice algal NPP averaged 1.7±1.5 g C m^{-2} yr^{-1} and was highly variable interannually, ranging between 0 and 4.4 g C m^{-2} yr^{-1} (Figure 6a). Between 1988 and 2018, IA NPP increased annually by 0.05 g C m^{-2} yr^{-1} ($R^2 = 0.101$, $p = 0.082$) and accounted for 0%–4.5% of total (phytoplankton + ice algae) annual NPP (mean = 1.9±1.6%; Table 4). Multiple linear regression revealed that 93.1% of the variance ($p<0.001$) in annual NPP by ice algae is controlled by the length of the snow melt period ($R^2 = 0.462$, $p<0.001$), ice thickness ($R^2 = 0.252$, $p<0.001$), and snow thickness ($R^2 = 0.216$, $p<0.001$).

NPP during the UI period varied from 0.6 to 73.9 g C m^{-2} yr^{-1} (mean = 44.3±22.6 g C m^{-2} yr^{-1}; Figure 6b), with no significant trend between 1988 and 2018. The UI period accounted for a mean of 48.7±22.0% of total annual NPP (range = 0.7%–78.2%; Table 4), the highest proportion among the four different periods. It also was the most important period for new production, with a mean of 35.8 g C m^{-2} yr^{-1} of new production (mean = 84.4% of UI NPP was new; Table S2). Surface waters were highly productive, with only 1.9% of UI NPP associated with an SCM (Table S3). One of the primary drivers of variation in UI NPP was UI period length; years with longer UI periods were associated with higher UI NPP ($R^2 = 0.818$, $p<0.001$; Figure 7a). Multiple linear regression revealed that 94.7% of the variance in UI NPP ($p<0.001$) is controlled by the length of the UI period ($R^2 = 0.545$, $p<0.001$), ice thickness ($R^2 = 0.347$, $p<0.001$), and the length of the snow melt period ($R^2 = 0.055$, $p<0.001$). Variation in UI NPP was the most important driver of interannual changes in total annual NPP ($R^2 = 0.424$, $p<0.001$).

In the MIZ period, NPP ranged from 3.0 to 55.9 g C m^{-2} yr^{-1} (mean = 20.1±15.6 g C m^{-2} yr^{-1}; Figure 6c) and accounted for 3.1%–66.5% of total annual NPP (mean = 23.6±19.1%; Table 4), with no interannual trend. The MIZ period was responsible for the smallest proportion of new production of the three periods,

Table 4
Bloom Type, % Ice Algal (IA), % UI, % MIZ, % OW, and Total NPP (g C m⁻² yr⁻¹) for Each Year

Year	Bloom Type	% IA	% UI	% MIZ	% OW	Total
1988	Mix	0.0	58.9	41.1	0.0	76.3
1989	UI	2.0	69.1	10.6	18.2	90.8
1990	Mix	1.9	43.0	20.0	35.1	82.1
1991	Mix	1.1	41.2	37.0	20.7	75.4
1992	Mix	0.0	38.4	29.0	32.6	74.7
1993	MIZ	2.1	2.1	60.7	35.0	89.4
1994	UI	3.8	78.2	8.3	9.7	94.2
1995	UI	0.0	67.5	15.0	17.4	95.6
1996	UI	3.1	66.0	10.2	20.7	100.1
1997	UI	2.0	59.9	11.2	27.0	86.4
1998	MIZ	0.0	1.4	64.4	34.2	86.2
1999	Mix	0.0	28.1	25.7	46.2	87.2
2000	Mix	0.2	30.7	43.0	26.1	77.4
2001	UI	3.2	62.0	11.8	23.0	84.9
2002	UI	2.7	71.3	3.1	22.9	96.7
2003	UI	3.4	66.4	13.3	16.9	95.6
2004	MIZ	2.2	5.7	66.5	25.6	84.0
2005	Mix	2.8	26.0	29.5	41.7	85.8
2006	UI	0.0	65.7	9.1	25.2	85.6
2007	UI	4.5	60.4	8.0	27.1	97.2
2008	UI	2.4	70.5	9.1	18.1	93.2
2009	UI	0.0	74.6	10.0	15.4	99.0
2010	MIZ	0.0	0.7	66.4	32.8	81.9
2011	UI	2.9	63.7	8.5	24.9	98.6
2012	Mix	0.0	46.5	27.0	27.5	81.1
2013	UI	3.4	70.0	7.3	19.3	99.7
2014	Mix	0.0	42.4	27.7	29.9	82.1
2015	UI	3.7	57.6	10.0	28.6	97.4
2016	Mix	2.9	40.2	21.2	35.7	83.4
2017	UI	3.9	46.9	13.1	35.7	83.4
2018	UI	3.9	55.4	13.4	27.3	98.8
Mean	UI	2.6±1.4	65.0±7.6	10.1±2.8	22.2±6.2	94.8±5.0
Mean	Mix	0.9±1.2	39.5±9.7	30.1±7.8	29.4±12.8	80.6±4.4
Mean	MIZ	1.1±1.2	2.5±2.2	64.5±2.7	31.9±4.3	85.4±3.2

Note. Annual cycles of net primary production (NPP) were separated into 3 clusters (Bloom Types): under ice dominated (UI), mixed dominance (Mix), and marginal ice zone dominated (MIZ). Means and standard deviation of the magnitude of total NPP (g C m⁻² yr⁻¹) and NPP within the UI, MIZ, and open water (OW) periods for each of the three clusters are listed at the bottom of the table.

accounting for only 13.6 g C m⁻² yr⁻¹ (mean = 60.0% of MIZ NPP was new; Table S2). During this period, the depth of maximum NPP transitioned from surface waters to the SCM, which accounted for 54.0% of MIZ NPP (Table S3). For all years except 1988 (when ice never retreated), the MIZ period length was significantly correlated with variation in MIZ NPP, with MIZ period length accounting for 40.4% of the variance in MIZ NPP ($p<0.001$; Figure 7a). Multiple linear regression for all years except 1988 revealed that 78.9% of the variance ($p<0.001$) in annual NPP in the MIZ is controlled by the lengths of the UI ($R^2 = 0.540$, $p<0.001$)
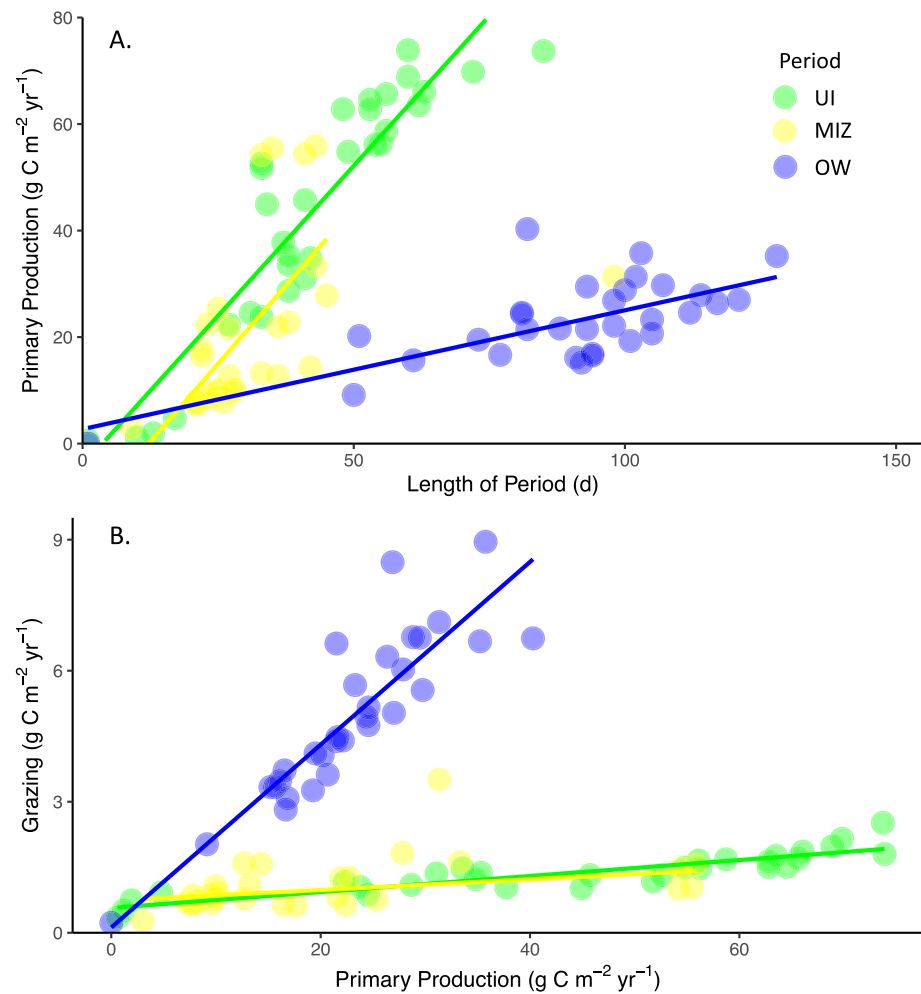
Figure 7. Scatterplots of (a) length of period (d) versus net primary production (NPP; g C m^{-2} yr^{-1}) and (b) NPP versus grazing (g C m^{-2} yr^{-1}) for the under-ice (UI; green), marginal ice zone (MIZ; yellow), and open water (OW; blue) periods. Lines (in the period color) are used when linear regressions are statistically significant.

and MIZ periods ($R^2 = 0.248$, $p = 0.002$). MIZ NPP was the second most important driver of interannual changes in annual NPP ($R^2 = 0.273$, $p = 0.003$).

NPP in the OW period varied from 9.1 to 40.3 g C m^{-2} yr^{-1} (mean = 23.6±2.9 g C m^{-2} yr^{-1}; Figure 6d) in the years when sea ice retreated (all years except 1988). OW NPP made up 9.7%–46.2% of annual NPP (mean = 26.7±8.2%, Table 4) but showed no interannual trend for years in which there was an OW period (1989–2018, $p = 0.185$). New production in the OW period averaged 17.4 g C m^{-2} yr^{-1} (mean = 77.2% of OW NPP was new production; Table S2). Most NPP during this period (mean = 94.4% of phytoplankton NPP) was associated with the SCM (Table S3). Variation in the length of the OW period was significantly correlated to the magnitude of OW NPP, with period length accounting for 47.4% of the variance in OW NPP (p <0.001; Figure 7a). Multiple linear regression revealed that 70.0% of the variance (p<0.001) in OW NPP was controlled by the lengths of the OW ($R^2 = 0.268$, p<0.001), UI ($R^2 = 0.237$, p<0.001), and MIZ ($R^2 = 0.081$, $p = 0.027$) periods and by sea ice thickness ($R^2 = 0.118$, $p = 0.059$). Variation in OW NPP did not significantly drive variation in total annual NPP.

Monthly integrated NPP also changed substantially between 1988 and 2018 (Figure 8), increasing annually by 0.005 g C m^{-2} yr^{-1} in March ($R^2 = 0.262$, $p = 0.003$), by 0.05 g C m^{-2} yr^{-1} in April ($R^2 = 0.213$, $p = 0.009$), and by 1.0 g C m^{-2} yr^{-1} in May ($R^2 = 0.190$, $p = 0.014$). In contrast, during the summer and autumn seasons, NPP decreased between 1988 and 2018. July NPP decreased by 0.41 g C m^{-2} yr^{-1} ($R^2 = 0.134$, $p = 0.043$)
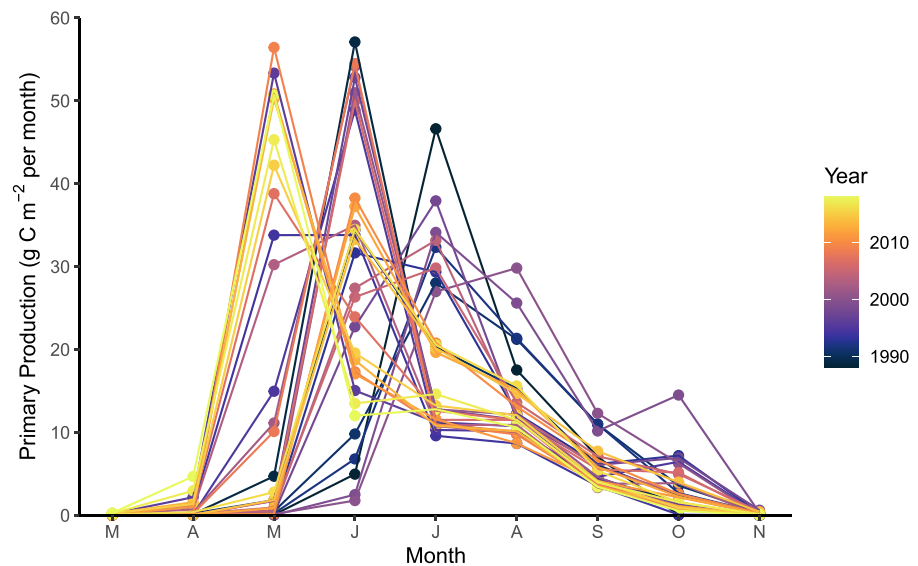
Figure 8. Monthly integrated water column net primary production (NPP; g C m^{-2} per month) for March–November from 1988 to 2018 (colorbar).

and September NPP by 0.09 g C m^{-2} yr^{-1} ($R^2 = 0.118$, $p = 0.059$). NPP during June, August, October, and November showed no significant trend over time.

3.4. Zooplankton Grazing

Zooplankton grazing of total annual NPP ranged from 4.9 to 11.1 g C m^{-2} yr^{-1} (mean = 7.5±1.4 g C m^{-2} yr^{-1}) and showed no trend with time.

During the UI period, grazing of NPP averaged 1.4±0.5 g C m^{-2} yr^{-1} (ranging between 0.3 and 2.5 g C m^{-2} yr^{-1} between 1988 and 2018), or 7.8±13.5% of UI NPP. Although there was no change in UI grazing between 1988 and 2018, it was significantly correlated to UI NPP, with 78.8% of variance in UI grazing attributable to annual changes in UI NPP ($p<0.001$, slope = 0.02 g C m^{-2} yr^{-1} yr^{-1}; Figure 7b). However, because high UI NPP depressed NPP in the MIZ and OW periods, UI NPP was negatively correlated with annual zooplankton grazing ($R^2 = 0.404$, $p<0.001$, slope = −0.040).

Grazing by zooplankton during the MIZ period averaged 1.1±0.6 g C m^{-2} yr^{-1} (ranging between 0.3 to 3.5 g C m^{-2} yr^{-1}), consuming 6.7±3.1% of MIZ NPP. 25.5% of the variance in zooplankton grazing during the MIZ period can be attributed to annual changes in MIZ NPP ($p = 0.004$, slope = 0.01 g C m^{-2} yr^{-1} yr^{-1}; Figure 7b). MIZ NPP was also correlated with total annual zooplankton grazing ($R^2 = 0.220$, $p = 0.008$, slope = 0.043).

Zooplankton grazing during the OW period varied between 1.7 and 9.0 g C m^{-2} yr^{-1} between 1989 and 2018 (mean = 5.1±1.7 g C m^{-2} yr^{-1}), or 21.4±3.5% of OW NPP, and didn't change significantly over time. OW NPP was significantly correlated with both grazing in the OW period ($R^2 = 0.726$, $p<0.001$, slope = 0.21 g C m^{-2} yr^{-1} yr^{-1}; Figure 7b) and annual grazing ($R^2 = 0.643$, $p<0.001$, slope = 0.144).

3.5. Water Column Bloom Types

Clustering analysis demonstrated that the annual cycle of NPP for each year could be separated into one of three different temporal patterns based on the periods defined above (Table 4): years where the UI bloom dominated total annual NPP (17 of 31 years; Figure 9a), years when the MIZ bloom dominated NPP (4 of 31 years; Figure 9c), and "mixed" years when both the UI and MIZ blooms were dominant (10 of 31 years; Figure 9b). For annual depth versus time plots for each of these three bloom types, see Section S5.4 and Figures S6–S8.
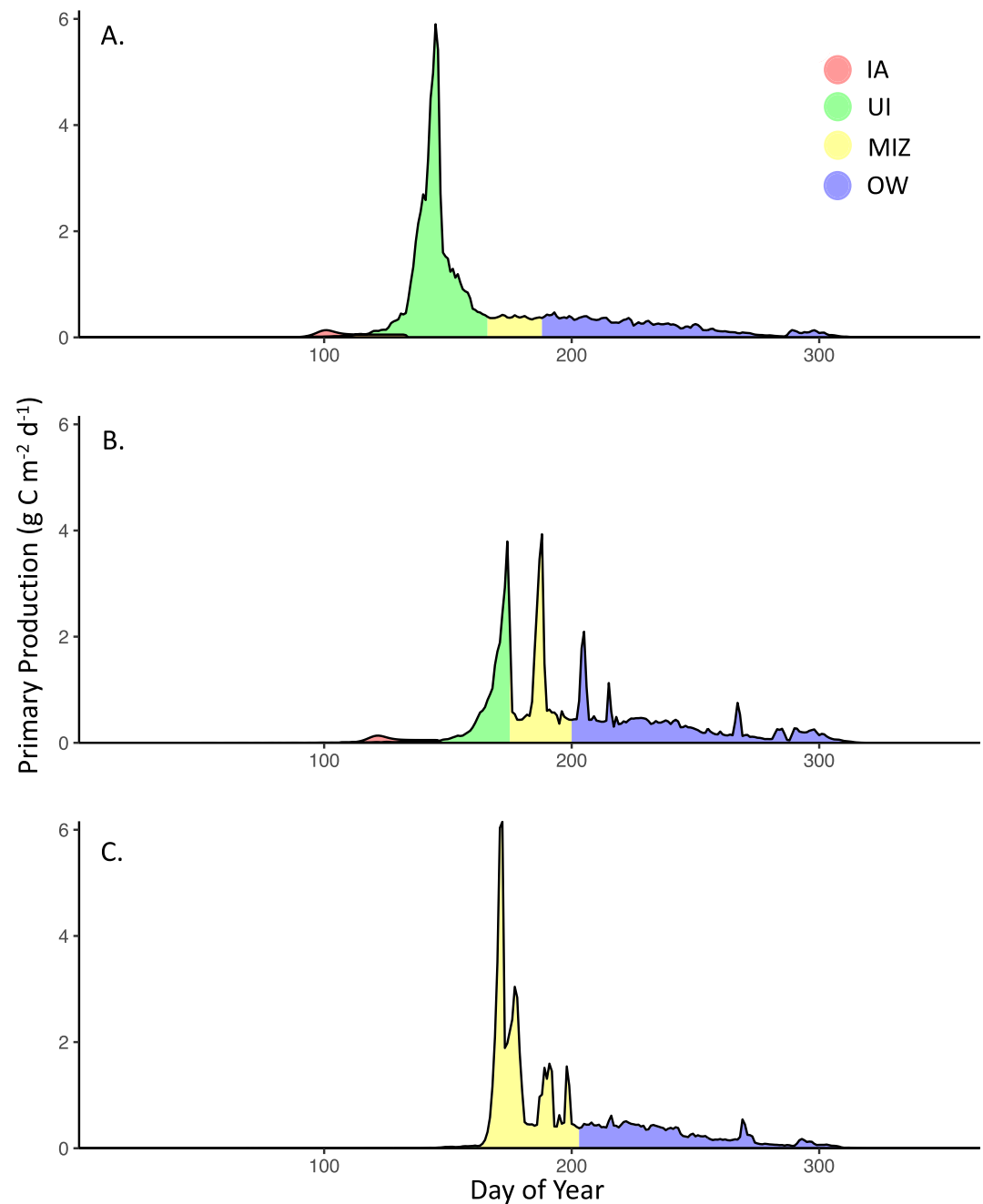
Figure 9. Example annual cycles of daily net primary production (NPP; g C m^{-2} d^{-1}) for (a) an under-ice (UI) dominant year (2013), (b) a year with mixed under-ice and marginal ice zone (MIZ) dominance (2005), and (c) an MIZ-dominant year (2010). Red shading represents production by ice algae (IA) while green, yellow, and blue shading represent production during UI, MIZ, and open water (OW) periods, respectively.

These bloom dominance types were associated with different magnitudes of total annual NPP and annual zooplankton grazing. UI-dominated blooms led to years with higher total annual NPP (94.8±5.0 g C m^{-2} yr^{-1}) than mixed (80.6±4.4 g C m^{-2} yr^{-1}, $p<0.001$) or MIZ-dominated blooms (85.4±3.2 g C m^{-2} yr^{-1}, $p = 0.003$). Total new production was also significantly higher in years dominated by UI blooms (71.3±3.4 g C m^{-2} yr^{-1}) than for mixed (64.5±3.2 g C m^{-2} yr^{-1}, $p<0.001$) or MIZ-dominant years (64.2±2.0 g C m^{-2} yr^{-1}, $p = 0.001$). There was no significant difference between peak daily NPP rate in UI-dominated blooms (5.1 ±1.6 g C m^{-2} d^{-1}) and mixed UI-MIZ blooms (4.1±0.7 g C m^{-2} d^{-1}). However, mixed dominance blooms

had, on average, lower peak production rates than MIZ-dominated blooms (6.3±1.4 g C m^{-2} d^{-1}, $p = 0.028$). Bloom type also affected the magnitude of annual zooplankton grazing ($p = 0.007$); UI-dominant years featured far less annual zooplankton grazing (7.1±1.1 g C m^{-2} yr^{-1}) than years with MIZ-dominant blooms (9.4±0.8 g C m^{-2} yr^{-1}). There was no difference in annual zooplankton grazing between mixed-dominance (7.6±1.6 g C m^{-2} yr^{-1}) and UI- or MIZ-dominant blooms.

There were no interannual trends in bloom type from 1988 to 2018, but environmental variables affected bloom type. The annual cycle was dominated by UI blooms under thinner ice conditions (1.68±0.28 m), while thicker ice resulted in either MIZ (2.40±0.19 m, $p<0.001$) or mixed-dominance blooms (2.50±0.07 m, $p< 0.001$). MIZ blooms dominated in years where ice retreated earlier (DOY 166.8±3.4 days), while mixed-dominance blooms formed when ice retreated later (DOY 187.9±10.7 days, $p = 0.019$).

4. Discussion

Despite its short growing season, the Chukchi Sea is a highly productive coastal ecosystem. Our model estimated a rate of total annual NPP ranging between 75 and 100 g C m^{-2} yr^{-1} between 1988 and 2018, values on the higher end of the 55–105 g C m^{-2} yr^{-1} of annual NPP previously reported for the Chukchi Sea (Arrigo et al., 2014; Hill & Cota, 2005; Lee et al., 2007). However, NPP in the Chukchi Sea can be patchy. Rates can surpass 170 g C m^{-2} yr^{-1} (Hansell et al., 1993; Hill, Ardyna, et al., 2018) along the NO$_3^-$-rich major advective pathways near our model study region but are typically much lower near the coast in the NO$_3^-$-deplete Alaska Coastal Current. Stabeno et al. (2020) argue that the high productivity of the Chukchi shelf is due to the existence of Multiple Productive Layers (the MPL hypothesis), whereby ice algae and phytoplankton contribute to high regional NPP in distinct surface and subsurface layers. Our study also partitions annual NPP, not by different layers, but rather into four periods of production in the Chukchi Sea: microalgae growing within sea ice and phytoplankton that bloom under sea ice, in the MIZ, and during the OW period.

Sea ice microalgae form the first source of NPP each year, and as a result, are a critical source of food to pelagic organisms (Arrigo, 2017; Fortier et al., 2002; Gradinger, 2009; Søreide et al., 2010) at a time of year when other sources of food are scarce (Assmy et al., 2013; Bradstreet & Cross, 1982). When light returns to the Chukchi Sea following the polar night, ice-associated algae are able to use their stable position atop the water column to take advantage of increasing under-ice light and high water column NO$_3^-$ concentrations. Ice algal concentrations can surpass 300 mg Chl a m^{-2}, although concentrations more typically range between 4 and 30 mg Chl a m^{-2} in the Chukchi Sea (Arrigo et al., 2017; Gradinger, 2009; Selz et al., 2018) and range between 0 and 30 mg Chl a in our model. These dense assemblages can substantially diminish the transmission of light through the ice, reducing light available to phytoplankton growing in the water column and further delaying the initiation of water column NPP. Ice algae modeled as a part of this study were able to grow under lower light conditions than phytoplankton, with algal blooms beginning on average 28 days earlier (and as much as 45 days earlier) than phytoplankton blooms. In addition to their importance as an early food source, ice algal assemblages are typically dominated by diatoms and can substantially contribute to annual C export (Boetius et al., 2013; Fahl & Nöthig, 2007) because their siliceous cell walls and large cell size cause them to sink rapidly through the water column (Smetacek, 1999). As a result, ice algal NPP is often thought to contribute substantially to the food available to benthic organisms (Campbell et al., 2009). In areas such as the central Arctic, ice algal NPP is thought to comprise more than 50% of total annual NPP. However, despite their importance to pelagic and benthic grazers and to C export, ice algae are probably minor contributors to total annual NPP in more productive parts of the Arctic, including the continental shelf of the Chukchi Sea. Mean annual ice algal NPP calculated in our model averaged 1.7 g C m^{-2} yr^{-1}, in line with previous observations of 1–2 g C m^{-2} (Gradinger, 2009) in the Chukchi Sea. As a result, modeled ice algal NPP contributed 0%–5% of total annual NPP in the Chukchi Sea, in line with the 2%–10% contribution estimated on Arctic continental shelves (Arrigo, 2017; Dupont, 2012; Gosselin et al., 1997; Jin et al., 2012).

The second period of production evaluated here, phytoplankton production in the under-ice period, was historically thought to be too light-limited to contribute substantially to annual NPP (Hameedi, 1978; Perrette et al., 2011). However, data from the ICESCAPE program (Arrigo et al., 2012, 2014) demonstrated that massive phytoplankton blooms can form beneath the sea ice. Light transmission through sea ice gradually

increases as snow melts, sea ice thins, ice algae slough off the bottom of the sea ice, and melt ponds proliferate on the surface of the ice (Light et al., 2015; Perovich & Polashenski, 2012). Phytoplankton, largely centric diatoms (Laney & Sosik, 2014) with high maximum photosynthetic rates and photosynthetic efficiencies (Lewis et al., 2019), are primed to bloom as light limitation lifts. Massive blooms have been reported in the UI period, with particularly extraordinary observations during the ICESCAPE 2011 cruise, where depth-integrated Chl a averaged a remarkable 840 mg m^{-2} over hundreds of km^2 of fully consolidated, 1 m thick sea ice (Arrigo et al., 2012, 2014). These high Chl a concentrations were also associated with high rates of NPP. During the ICESCAPE 2011 cruise, the UI period alone was found to contribute nearly 70 g C m^{-2} yr^{-1} (Arrigo et al., 2014), comparable to our modeled annual rates of UI NPP, which were 62.8 g C m^{-2} yr^{-1} in 2011 and the maximum for the time series, 73.9 g C m^{-2} yr^{-1} in 2009. Our model results further suggest that UI NPP accounted for nearly half of total annual NPP between 1988 and 2018, and years in which UI blooms dominated saw, on average, higher total annual NPP. The importance of the UI period to annual NPP is supported by a number of recent studies, which have found that NPP associated with UIBs was of equal or greater magnitude to NPP in the rest of the year (Arrigo et al., 2014; Lowry et al., 2014; Mayot et al., 2018; Mundy et al., 2009; Oziel et al., 2019). Despite growing evidence of the high rates of NPP during the UI period, the fate of UI NPP remains under-studied. Because the mixed layer remains cold (<−1.5°C) during the UI period, previous studies have found that zooplankton species were unable to graze effectively (Campbell et al., 2001; Coyle et al., 2007; Huntley & Lopez, 1992), possibly leading to a mismatch in phytoplankton and zooplankton annual cycles (Conover & Huntley, 1991). Our results indicate that UI-period zooplankton grazing scarcely increased in years with high UI NPP, indicating that low temperatures prevented zooplankton from taking advantage of increased food availability in the UI period. Further, years with high UI NPP were associated with reduced annual zooplankton grazing. Consequently, increasing NPP in the UI period may intensify the mismatch in phytoplankton and zooplankton (Conover & Huntley, 1991), increasing organic matter export to the sediments (Lalande et al., 2020) and thus decreasing food availability to pelagic-feeding fish, birds, and mammals (Bradstreet & Cross, 1982; Loeng et al., 2005).

More frequent observations of UIBs in recent years (Ardyna et al., 2020) and model results by Horvat et al. (2017) lend credence to the hypothesis that changing ice conditions have led to an increased incidence of UIBs in recent years (Arrigo et al., 2014). However, our model demonstrates that, as early as 1988, conditions in the northern Chukchi Sea were amenable to UIB formation. The UI period was, in fact, the most productive period in 17 of the 31 years modeled as a part of this study and was only insubstantial (UI NPP of < 5 g C m^{-2} yr^{-1}) in four years with thick sea ice cover. While our study found a substantial increasing trend in total annual NPP during spring (1.1 g C m^{-2} yr^{-1}) between 1988 and 2018, we found no evidence of increasing NPP associated with the UI period over this timeframe. This is likely a function of the location we chose to model, which is a region where multi-year ice is present in some years but not others. The associated high degree of interannual variability in sea ice age and thickness resulted in highly variable NPP during the UI period, which swamped any secular trend over time. Had we elected to model a region further to the south that was dominated by first year ice, rather than the site of the massive UIB observed during ICESCAPE 2011 (Arrigo et al., 2012), we likely would have observed an increase in UI NPP between 1988 and 2018.

The MIZ period, representing the third source of production evaluated as a part of our study, has been historically associated with the highest rates of NPP in Arctic waters (Niebauer, 1991; Perrette et al., 2011; Sakshaug, 2004). As ice breaks up and retreats within the MIZ, the mixed layer shoals substantially, dramatically increasing light available in the water column and allowing for rapid phytoplankton growth (Sakshaug & Skjoldal, 1989) that strips nutrients from the mixed layer (Perrette et al., 2011). Using satellite observations, Perrette et al. (2011) noted that high Chl a concentrations can be found in a narrow band (20–100 km) along the ice edge, moving northward as ice retreats. Although the MIZ blooms only last 20 days following sea ice retreat in the analysis of Perrette et al. (2011), their study estimates that rates of MIZ NPP were up to twice as high as during the OW period. However, our study found that, while the MIZ period could contribute substantially to total annual NPP in years with particularly thick multi-year sea ice, on average it accounted for the smallest proportion (less than 24%) of total NPP between 1988 and 2018 of the three pelagic sources of NPP evaluated. Further, we found that this period accounted for a mere 10% of total NPP in years characterized by large UIBs. During most years from 1988-2018, the MIZ period represented a transition as NPP shifted from NO_3^--depleted surface waters down to the SCM. As a result, the MIZ period generated a smaller

proportion of new production than either the UI or the OW periods. Much of the discrepancy between our findings and those of Perrette et al. (2011) can be attributed to the fact that Perrette et al. (2011) assumed that all Chl a observed in the 20 days following sea ice retreat was generated in the MIZ, ignoring the possibility of UI generation of production. Lowry et al. (2014) considered locations in the Chukchi Sea to host MIZ blooms if Chl a increased following ice retreat, but were likely to host UIBs if Chl a concentrations decreased. Their study suggested that UIBs covered an area 2.5-fold higher than blooms generated in the MIZ between 1998 and 2012. While NPP in the MIZ period is more easily studied than in the UI period, our study found that the MIZ period is likely not as important in driving annual NPP in the Chukchi Sea as the UI period.

During the OW period, the fourth NPP source evaluated here, phytoplankton productivity is largely confined to the SCM (Arrigo et al., 2014; Brown et al., 2015; Hill & Cota, 2005; Martin et al., 2010). UI and MIZ NPP leaves surface waters devoid of NO_3^-, preventing substantial surface NPP in the OW period (Codispoti et al., 2005, 2009; Mills et al., 2018). As a result, most phytoplankton biomass in this period is concentrated in a layer just below the mixed layer, where NO_3^- concentrations remain elevated and light is still available (Brown et al., 2015; Hill & Cota, 2005). While diatoms dominate community composition in the SCM (Hill & Cota, 2005), small flagellates can become abundant in surface waters following NO_3^- depletion (Li et al., 2009). Our study showed that greater than 90% of OW NPP was located within the SCM. In a study of SCMs in the Chukchi Sea between 2002 and 2012, Brown et al. (2015) found that SCMs developed up to one month prior to ice retreat, and gradually deepen to ~30 m by the summer. Consistent with these observations, we find that SCMs can be generated as much as 34 days before ice retreat in years with UIBs. The generation of an SCM during the UI period supports the hypothesis, first put forth by Palmer et al. (2013) and Brown et al. (2015), that phytoplankton growing in the low-light conditions of the UI period are better photophysiologicaly acclimated to grow once they descend to the SCM.

While the MIZ and OW periods have historically been presumed to be far more productive on Arctic continental shelves than the ice-covered portion of the year, our study demonstrates that UI production makes up the greatest proportion of total annual NPP in the northern Chukchi Sea and is the most critical period in driving interannual variability. Relying on cruise and satellite data exclusively from the MIZ and OW periods has historically caused us to drastically underestimate NPP in parts of the Arctic that host UIBs. A satellite-based survey by Arrigo and Van Dijken (2011), for example, estimated that annual NPP between 1998 and 2008 was only 5 g C m^{-2} yr^{-1} at the location of this model, more than an order of magnitude lower than both the Arrigo et al. (2014) NPP estimates based on nitrate drawdown and our modeled estimates of total annual NPP. Incorporation of new technologies that allow us to better estimate the relative importance of UIBs to total annual NPP, such as moorings, floats, or AUVs with bio-optical or biogeochemical sensors, are more likely to produce accurate estimates of regional NPP.

Further, our study finds that conditions in the Chukchi Sea have likely been amenable to the formation of UIBs since at least the late 1980s. Indeed, observations of UIBs dating back to at least 1957 (English, 1961) indicate that UIBs have been generated sporadically for decades. However, as thinner, younger sea ice has come to dominate much of the Arctic Ocean in recent years (Laxon et al., 2013; Serreze & Stroeve, 2015), observations of UIBs have grown to include most of the Arctic Ocean (Ardyna et al., 2020). It is quite likely that continued changes in sea ice cover will only make UIBs more widespread in the Arctic Ocean in the future (Horvat et al., 2017), further demonstrating the critical importance of better understanding NPP under sea ice.

Data Availability Statement

Model code and all data are available at https://purl.stanford.edu/gc896jc5127.

References

Anderson, M., Bliss, A., & Drobot, S. (2019). *Snow melt onset over Arctic Sea ice from SMMR and SSM/I-SSMIS brightness temperatures*. NASA National Snow and Ice Data Center DAAC. https://doi.org/10.5067/A9YK15H5EBHK

Apollonio, S., & Matrai, P. (2011). Marine primary production in the Canadian Arctic, 1956, 1961–1963. *Polar Biology*, *34*(5), 767–774. https://doi.org/10.1007/s00300-010-0928-3

Ardyna, M., Babin, M., Gosselin, M., Devred, E., Rainville, L., & Tremblay, J. (2014). Recent Arctic Ocean sea ice loss triggers novel fall phytoplankton blooms. *Geophysical Research Letters*, *41*, 6207–6212. https://doi.org/10.1002/2014GL061047.Received

Ardyna, M., Mundy, C. J., Mayot, N., Matthes, L. C., Oziel, L., Horvat, C., et al. (2020). Under-ice phytoplankton blooms: Shedding light on the "invisible" part of Arctic primary production. *Frontiers in Marine Science*, *7*, 608032. https://doi.org/10.3389/fmars.2020.608032

Arrigo, K. R. (2017). Sea ice as a habitat for primary producers. In D. N. Thomas (Ed.), Sea Ice (pp. 352–369). John Wiley & Sons, Ltd. https://doi.org/10.1002/9781118778371.ch14

Arrigo, K. R., Mills, M., van Dijken, G., Lowry, K., Pickart, R., & Schlitzer, R. (2017). Late spring nitrate distributions beneath the ice-covered northeastern Chukchi Shelf. *Journal of Geophysical Research: Biogeosciences*, *122*, 2409–2417. https://doi.org/10.1002/2017JG003881

Arrigo, K. R., Perovich, D. K., Pickart, R. S., Brown, Z. W., van Dijken, G. L., Lowry, K. E., et al. (2012). Massive phytoplankton blooms under Arctic Sea Ice. *Science*, *336*, 1408–1408. https://doi.org/10.1126/science.1215065

Arrigo, K. R., Perovich, D. K., Pickart, R. S., Brown, Z. W., van Dijken, G. L., Lowry, K. E., et al. (2014). Phytoplankton blooms beneath the sea ice in the Chukchi Sea. *Deep-Sea Research Part II: Topical Studies in Oceanography*, *105*, 1–16. https://doi.org/10.1016/j.dsr2.2014.03.018

Arrigo, K. R., Sullivan, C. W., & Kremer, J. N. (1991). A bio-optical model of Antarctic sea ice. *Journal of Geophysical Research*, *96*(C6), 10581–10592. https://doi.org/10.1029/91JC00455

Arrigo, K. R., van Dijken, G., & Pabi, S. (2008). Impact of a shrinking Arctic ice cover on marine primary production. *Geophysical Research Letters*, *35*(August), 1–6. https://doi.org/10.1029/2008GL035028

Arrigo, K. R., & Van Dijken, G. L. (2011). Secular trends in Arctic Ocean net primary production. *Journal of Geophysical Research*, *116*(9), 1–15. https://doi.org/10.1029/2011JC007151

Arrigo, K. R., Worthen, D., Schnell, A., & Lizotte, M. (1998). Primary production in Southern Ocean waters. *Journal of Geophysical Research*, *103*(C8), 15587–15600. https://doi.org/10.1029/98JC00930

Arrigo, K. R., Worthen, D. L., & Robinson, D. H. (2003). A coupled ocean-ecosystem model of the Ross Sea: 2. Iron regulation of phytoplankton taxonomic variability and primary production. *Journal of Geophysical Research*, *108*(C7), 3231–3231. https://doi.org/10.1029/2001JC000856

Ashjian, C. J., Campbell, R. G., Welch, H. E., Butler, M., & Van Keuren, D. (2003). Annual cycle in abundance, distribution, and size in relation to hydrography of important copepod species in the western Arctic Ocean. *Deep-Sea Research Part I: Oceanographic Research Papers*, *50*(10–11), 1235–1261. https://doi.org/10.1016/S0967-0637(03)00129-8

Assmy, P., Ehn, J. K., Fernández-Méndez, M., Hop, H., Katlein, C., Sundfjord, A., et al. (2013). Floating ice-algal aggregates below melting Arctic Sea Ice. *PloS One*, *8*(10), e76599. https://doi.org/10.1371/journal.pone.0076599

Assmy, P., Fernández-Méndez, M., Duarte, P., Meyer, A., Randelhoff, A., Mundy, C. J., et al. (2017). Leads in Arctic pack ice enable early phytoplankton blooms below snow-covered sea ice. *Scientific Reports*, *7*(1), 40850. https://doi.org/10.1038/srep40850

Boetius, A., Albrecht, S., Bakker, K., Bienhold, C., Felden, J., Fernandez-Mendez, M., et al. (2013). Export of algal biomass from the melting Arctic Sea Ice. *Science*, *339*(6126), 1430–1432. https://doi.org/10.1126/science.1231346

Boles, E., Provost, C., Garçon, V., Bertosio, C., Athanase, M., Koenig, Z., & Sennéchael, N. (2020). Under-ice phytoplankton blooms in the central Arctic Ocean: Insights from the first biogeochemical IAOOS platform drift in 2017. *Journal of Geophysical Research: Oceans*, *125*(3). https://doi.org/10.1029/2019JC015608

Bradstreet, M. S., & Cross, W. E. (1982). Trophic relationships at high Arctic ice edges. *Arctic*, *35*(1), 1–12. https://doi.org/10.14430/arctic2303

Bricaud, A., Babin, M., Morel, A., & Claustre, H. (1995). Variability in the chlorophyll-specific absorption coefficients of natural phytoplankton: Analysis and parameterization. *Journal of Geophysical Research*, *100*(C7), 13321–13332. https://doi.org/10.1029/95JC00463

Brown, Z. W., Lowry, K. E., Palmer, M. A., van Dijken, G. L., Mills, M. M., Pickart, R. S., & Arrigo, K. R. (2015). Characterizing the subsurface chlorophyll a maximum in the Chukchi Sea and Canada Basin. *Deep-Sea Research Part II: Topical Studies in Oceanography*, *118*, 88–104. https://doi.org/10.1016/j.dsr2.2015.02.010

Brzezinski, M. A. (1985). The Si:C:N ratio of marine diatoms: Interspecific variability and the effect of some environmental variables. *Journal of Phycology*, *21*(3), 347–357.

Burchard, H., Bolding, K., & Ruiz-Villarreal, M. (1999). *GOTM, a general ocean turbulence model. Theory, implementation and test cases*. Space Applications Institute.

Campbell, R. G., Sherr, E. B., Ashjian, C. J., Plourde, S., Sherr, B. F., Hill, V. J., & Stockwell, D. A. (2009). Mesozooplankton prey preference and grazing impact in the western Arctic Ocean. *Deep Sea Research Part II: Topical Studies in Oceanography*, *56*(17), 1274–1289. https://doi.org/10.1016/j.dsr2.2008.10.027

Campbell, R. G., Wagner, M., Teegarden, G., Boudreau, C., & Durbin, E. (2001). Growth and development rates of the copepod Calanus finmarchicus reared in the laboratory. *Marine Ecology Progress Series*, *221*, 161–183. https://doi.org/10.3354/meps221161

Codispoti, L. A., Flagg, C., Kelly, V., & Swift, J. H. (2005). Hydrographic conditions during the 2002 SBI process experiments. *Deep-Sea Research Part II: Topical Studies in Oceanography*, *52*(24–26), 3199–3226. https://doi.org/10.1016/j.dsr2.2005.10.007

Codispoti, L. A., Flagg, C. N., & Swift, J. H. (2009). Hydrographic conditions during the 2004 SBI process experiments. *Deep-Sea Research II*, *56*, 1144–1163. https://doi.org/10.1016/j.dsr2.2008.10.013

Comiso, J. C. (2012). Large decadal decline of the arctic multiyear ice cover. *Journal of Climate*, *25*(4), 1176–1193. https://doi.org/10.1175/JCLI-D-11-00113.1

Conover, R., & Huntley, M. (1991). Copepods in ice-covered seas—Distribution, adaptations to seasonally limited food, metabolism, growth patterns and life cycle strategies in polar seas. *Journal of Marine Systems*, *2*(1–2), 1–41. https://doi.org/10.1016/0924-7963(91)90011-I

Cooper, L. W., & Grebmeier, J. M. (2018). Deposition patterns on the Chukchi shelf using radionuclide inventories in relation to surface sediment characteristics. *Deep Sea Research Part II: Topical Studies in Oceanography*, *152*, 48–66. https://doi.org/10.1016/j.dsr2.2018.01.009

Corlett, W. B., & Pickart, R. S. (2017). Progress in oceanography the Chukchi slope current. *Progress in Oceanography*, *153*, 50–65. https://doi.org/10.1016/j.pocean.2017.04.005

Cota, G., & Home, E. (1989). Physical control of arctic ice algal production. *Marine Ecology Progress Series*, *52*, 111–121. https://doi.org/10.3354/meps052111

Coyle, K., Konar, B., Blanchard, A., Highsmith, R., Carroll, J., Carroll, M., & Sirenko, B. (2007). Potential effects of temperature on the benthic infaunal community on the southeastern Bering Sea shelf: Possible impacts of climate change. *Deep Sea Research Part II: Topical Studies in Oceanography*, *54*(23–26), 2885–2905. https://doi.org/10.1016/j.dsr2.2007.08.025

Darby, D., Ortiz, J., Polyak, L., Lund, S., Jakobsson, M., & Woodgate, R. (2009). The role of currents and sea ice in both slowly deposited central Arctic and rapidly deposited Chukchi–Alaskan margin sediments. *Global and Planetary Change*, *68*(1–2), 58–72. https://doi.org/10.1016/j.gloplacha.2009.02.007

Davis, J., & Benner, R. (2007). Quantitative estimates of labile and semi-labile dissolved organic carbon in the western Arctic Ocean: A molecular approach. *Limnology and Oceanography*, *52*(6), 2434–2444. https://doi.org/10.4319/lo.2007.52.6.2434

Dobson, F. W., & Smith, S. D. (1988). Bulk models of solar radiation at sea. *Quarterly Journal of the Royal Meteorological Society*, *114*(479), 165–182. https://doi.org/10.1002/qj.49711447909

Dupont, F. (2012). Impact of sea-ice biology on overall primary production in a biophysical model of the pan-Arctic Ocean: Arctic ice-ocean bio-physical model. *Journal of Geophysical Research*, *117*(C8). https://doi.org/10.1029/2011JC006983

English, T. (1961). Some biological observations in the central north polar sea drift station alpha, 1957-1958. *Scientific Reports* No, *15*, 1–80.

Eppley, R. W. (1972). Temperature and Phytoplankton Growth in the Sea. *Fishery Bulletin*, *70*(4), 1063–1085.

Fahl, K., & Nöthig, E.-M. (2007). Lithogenic and biogenic particle fluxes on the Lomonosov Ridge (central Arctic Ocean) and their relevance for sediment accumulation: Vertical vs. lateral transport. *Deep Sea Research Part I: Oceanographic Research Papers*, *54*(8), 1256–1272. https://doi.org/10.1016/j.dsr.2007.04.014

Fasham, M. J. R., Ducklow, H. W., & McKelvie, S. M. (1990). A nitrogen-based model of plankton dynamics in the oceanic mixed layer. *Journal of Marine Research*, *48*(3), 591–639. https://doi.org/10.1357/002224090784984678

Fortier, M., Fortier, L., Michel, C., & Legendre, L. (2002). Climatic and biological forcing of the vertical flux of biogenic particles under seasonal Arctic sea ice. *Marine Ecology Progress Series*, *225*, 1–16. https://doi.org/10.3354/meps225001

Gosselin, M., Levasseur, M., Wheeler, P. A., Horner, R. A., & Booth, B. C. (1997). New measurements of phytoplankton and ice algal production in the Arctic Ocean. *Deep Sea Research Part II: Topical Studies in Oceanography*, *44*(8), 1623–1644. https://doi.org/10.1016/S0967-0645(97)00054-4

Gradinger, R. (2009). Sea-ice algae: Major contributors to primary production and algal biomass in the Chukchi and Beaufort Seas during May/June 2002. *Deep Sea Research Part II: Topical Studies in Oceanography*, *56*(17), 1201–1212. https://doi.org/10.1016/j.dsr2.2008.10.016

Gregg, W. W., & Carder, K. L. (1990). A simple spectral solar irradiance model for cloudless maritime atmospheres. *Limnology and Oceanography*, *35*(8), 1657–1675. https://doi.org/10.4319/lo.1990.35.8.1657

Hameedi, M. J. (1978). Aspects of water column primary productivity in the Chukchi Sea during summer. *Marine Biology*, *48*(1), 37–46. https://doi.org/10.1007/BF00390529

Hansell, D. A., Whitledge, T. E., & Goering, J. J. (1993). Patterns of nitrate utilization and new production over the Bering-Chukchi shelf. *Continental Shelf Research*, *13*(5–6), 601–627. https://doi.org/10.1016/0278-4343(93)90096-G

Hill, V. J., Ardyna, M., Lee, S. H., & Varela, D. E. (2018). Decadal trends in phytoplankton production in the Pacific Arctic Region from 1950 to 2012. *Deep Sea Research Part II: Topical Studies in Oceanography*, *152*, 82–94. https://doi.org/10.1016/j.dsr2.2016.12.015

Hill, V. J., & Cota, G. (2005). Spatial patterns of primary production on the shelf, slope and basin of the Western Arctic in 2002. *Deep-Sea Research Part II: Topical Studies in Oceanography*, *52*(24–26), 3344–3354. https://doi.org/10.1016/j.dsr2.2005.10.001

Hill, V. J., Light, B., Steele, M., & Zimmerman, R. C. (2018). Light availability and phytoplankton growth beneath Arctic Sea Ice: Integrating observations and modeling. *Journal of Geophysical Research: Oceans*, *123*(5), 3651–3667. https://doi.org/10.1029/2017JC013617

Horvat, C., Jones, D. R., Iams, S., Schroeder, D., Flocco, D., & Feltham, D. (2017). The frequency and extent of sub-ice phytoplankton blooms in the Arctic Ocean. *Science Advances*, *3*(3), e1601191. https://doi.org/10.1126/sciadv.1601191

Huntley, M., & Lopez, M. (1992). Temperature-dependent production of marine copepods: A Global Synthesis. *The American Naturalist*, *140*(2), 201–242. https://doi.org/10.1086/285410

Jin, M., Deal, C., Lee, S. H., Elliott, S., Hunke, E., Maltrud, M., & Jeffery, N. (2012). Investigation of Arctic sea ice and ocean primary production for the period 1992–2007 using a 3-D global ice–ocean ecosystem model. *Deep Sea Research Part II: Topical Studies in Oceanography*, *81–84*, 28–35. https://doi.org/10.1016/j.dsr2.2011.06.003

Kondo, J. (1975). Air-sea bulk transfer coefficients in diabatic conditions. *Boundary-Layer Meteorology*, *9*(1), 91–112. https://doi.org/10.1007/BF00232256

Lalande, C., Grebmeier, J. M., Hopcroft, R. R., & Danielson, S. L. (2020). Annual cycle of export fluxes of biogenic matter near Hanna Shoal in the northeast Chukchi Sea. *Deep Sea Research Part II: Topical Studies in Oceanography*, *177*, 104730. https://doi.org/10.1016/j.dsr2.2020.104730

Laney, S. R., & Sosik, H. M. (2014). Phytoplankton assemblage structure in and around a massive under-ice bloom in the Chukchi Sea. *Deep Sea Research Part II: Topical Studies in Oceanography*, *105*, 30–41. https://doi.org/10.1016/j.dsr2.2014.03.012

Laxon, S. W., Giles, K. A., Ridout, A. L., Wingham, D. J., Willatt, R., Cullen, R., et al. (2013). CryoSat-2 estimates of Arctic sea ice thickness and volume. *Geophysical Research Letters*, *40*(4), 732–737. https://doi.org/10.1002/grl.50193

Lee, S. H., Whitledge, T. E., & Kang, S.-H. (2007). Recent carbon and nitrogen uptake rates of phytoplankton in Bering Strait and the Chukchi Sea. *Continental Shelf Research*, *27*(17), 2231–2249. https://doi.org/10.1016/j.csr.2007.05.009

Leu, E., Søreide, J., Hessen, D., Falk-Petersen, S., & Berge, J. (2011). Consequences of changing sea-ice cover for primary and secondary producers in the European Arctic shelf seas: Timing, quantity, and quality. *Progress in Oceanography*, *90*(1–4), 18–32. https://doi.org/10.1016/j.pocean.2011.02.004

Lewis, K. M., Arntsen, A. E., Coupel, P., Joy-Warren, H., Lowry, K. E., Matsuoka, A., et al. (2019). Photoacclimation of Arctic Ocean phytoplankton to shifting light and nutrient limitation. *Limnology and Oceanography*, *64*(1), 284–301. https://doi.org/10.1002/lno.11039

Lewis, K. M., & Arrigo, K. R. (2020). Ocean color algorithms for estimating chlorophyll *a*, CDOM absorption, and particle backscattering in the Arctic Ocean. *Journal of Geophysical Research: Oceans*, *125*(6). https://doi.org/10.1029/2019JC015706

Lewis, K. M., van Dijken, G. L., & Arrigo, K. R. (2020). Changes in phytoplankton concentration now drive increased Arctic Ocean primary production. *Science*, *369*(6500), 198–202. https://doi.org/10.1126/science.aay8380

Li, W. K., McLaughlin, F. A., Lovejoy, C., & Carmack, E. C. (2009). Smallest algae thrive as the Arctic Ocean freshens. *Science*, *326*(5952), 539–539. https://doi.org/10.1126/science.1179798

Light, B., Perovich, D. K., Webster, M. A., Polashenski, C., & Dadic, R. (2015). Optical properties of melting first-year Arctic sea ice. *Journal of Geophysical Research: Oceans*, *120*(11), 7657–7675. https://doi.org/10.1002/2015JC011163

Liston, G. E., Itkin, P., Stroeve, J., Tschudi, M., Stewart, J. S., Pedersen, S. H., & Elder, K. (2020). A Lagrangian snow-evolution system for sea-ice applications (SnowModel-LG): Part I—model description. *Journal of Geophysical Research: Oceans*, *43*, e2019JC015913.

Loeng, H., Brander, K., Carmack, E., Denisenko, S., Drinkwater, K., Hansen, B., & Sakshaug, E. (2005). *Marine systems. Arctic climate impact assessment*.

Lomas, M. W., Baer, S. E., Acton, S., & Krause, J. W. (2019). Pumped Up by the Cold: Elemental Quotas and Stoichiometry of Cold-Water Diatoms. *Frontiers in Marine Science*, *6*, 286. https://doi.org/10.3389/fmars.2019.00286

Lowry, K. E., Pickart, R. S., Mills, M. M., Brown, Z. W., Dijken, G. L. V., Bates, N. R., & Arrigo, K. R. (2015). The influence of winter water on phytoplankton blooms in the Chukchi Sea. *Deep-Sea Research Part II*, *118*, 53–72. https://doi.org/10.1016/j.dsr2.2015.06.006

Lowry, K. E., van Dijken, G. L., & Arrigo, K. R. (2014). Evidence of under-ice phytoplankton blooms in the Chukchi Sea from 1998 to 2012. *Deep-Sea Research Part II: Topical Studies in Oceanography*, *105*, 105–117. https://doi.org/10.1016/j.dsr2.2014.03.013

Martin, J., Tremblay, J., Gagnon, J., Tremblay, G., Lapoussière, A., Jose, C., et al. (2010). Prevalence, structure and properties of subsurface chlorophyll maxima in Canadian Arctic waters. *Marine Ecology Progress Series*, *412*, 69–84. https://doi.org/10.3354/meps08666

Mauritzen, C. (2012). Arctic freshwater. *Nature Geoscience*, *5*(3), 162–164. https://doi.org/10.1038/ngeo1409

Mayot, N., Matrai, P., Ellingsen, I. H., Steele, M., Johnson, K., Riser, S. C., & Swift, D. (2018). Assessing phytoplankton activities in the seasonal ice zone of the Greenland Sea over an annual cycle. *Journal of Geophysical Research: Oceans*, *123*(11), 8004–8025. https://doi.org/10.1029/2018JC014271

McMinn, A., Ashworth, C., & Ryan, K. (1999). Growth and productivity of Antarctic Sea ice algae under PAR and UV irradiances. *Botanica Marina*, *42*(4). https://doi.org/10.1515/BOT.1999.046

Meier, W. N., Fetterer, F., Savoie, M., Mallory, S., Duerr, R., & Stroeve, J. (2019). *NOAA/NSIDC climate data record of passive microwave sea ice concentration*. Version 3. NSIDC: National Snow and Ice Data Center. https://doi.org/10.7265/N59P2ZTG

Mills, M. M., Brown, Z. W., Laney, S. R., Ortega-Retuerta, E., Lowry, K. E., van Dijken, G. L., & Arrigo, K. R. (2018). Nitrogen limitation of the summer phytoplankton and heterotrophic prokaryote communities in the Chukchi Sea. *Frontiers in Marine Science*, *5*, 362. https://doi.org/10.3389/fmars.2018.00362

Mordy, C. W., Bell, S., Cokelet, E. D., Ladd, C., Lebon, G., Proctor, P., et al. (2020). Seasonal and interannual variability of nitrate in the eastern Chukchi Sea: Transport and winter replenishment. *Deep sea research part II: Topical Studies in Oceanography*, *177*, 104807. https://doi.org/10.1016/j.dsr2.2020.104807

Morel, A. (1978). Available, usable, and stored radiant energy in relation to marine photosynthesis. *Deep-Sea Research*, *25*(8), 673–688. https://doi.org/10.1016/0146-6291(78)90623-9

Mundy, C. J., Gosselin, M., Ehn, J., Gratton, Y., Rossnagel, A., Barber, D. G., et al. (2009). Contribution of under-ice primary production to an ice-edge upwelling phytoplankton bloom in the Canadian Beaufort Sea. *Geophysical Research Letters*, *36*(17), L17601. https://doi.org/10.1029/2009GL038837

Mundy, C. J., Gosselin, M., Gratton, Y., Brown, K., Galindo, V., Campbell, K., et al. (2014). Role of environmental factors on phytoplankton bloom initiation under landfast sea ice in Resolute Passage, Canada. *Marine Ecology Progress Series*, *497*, 39–49. https://doi.org/10.3354/meps10587

Niebauer, H. (1991). Bio-physical oceanographic interactions at the edge of the Arctic ice pack. *Journal of Marine Systems*, *2*(1–2), 209–232. https://doi.org/10.1016/0924-7963(91)90025-P

Oziel, L., Massicotte, P., Randelhoff, A., Ferland, J., Vladoiu, A., Lacour, L., et al. (2019). Environmental factors influencing the seasonal dynamics of spring algal blooms in and beneath sea ice in western Baffin Bay. *Elementa: Science of the Anthropocene*, *7*, 34. https://doi.org/10.1525/elementa.372

Pabi, S., van Dijken, G. L., & Arrigo, K. R. (2008). Primary production in the Arctic Ocean, 1998-2006. *Journal of Geophysical Research*, *113*(8), 1–22. https://doi.org/10.1029/2007JC004578

Pacini, A., Moore, G. W. K., Pickart, R. S., Nobre, C., Bahr, F., Våge, K., & Arrigo, K. R. (2019). Characteristics and transformation of Pacific winter water on the Chukchi Sea shelf in late spring. *Journal of Geophysical Research: Oceans*, *124*(10), 7153–7177. https://doi.org/10.1029/2019JC015261

Palmer, M. A., van Dijken, G. L., Mitchell, B. G., Seegers, B. J., Lowry, K. E., Mills, M. M., & Arrigo, K. R. (2013). Light and nutrient control of photosynthesis in natural phytoplankton populations from the Chukchi and Beaufort seas, Arctic Ocean. *Limnology and Oceanography*, *58*(6), 2185–2205. https://doi.org/10.4319/lo.2013.58.6.2185

Peng, G., Meier, W. N., Scott, D. J., & Savoie, M. H. (2013). A long-term and reproducible passive microwave sea ice concentration data record for climate studies and monitoring. *Earth System Science Data*, *8*. https://doi.org/10.5194/essd-5-311-2013

Perovich, D. K., Maykut, G. A., & Grenfell, T. C. (1986). Optical Properties of ice and snow in the polar oceans. I: Observations. In M. A. Blizard (Ed.), Technical symposium southeast (p. 232). https://doi.org/10.1117/12.964238

Perovich, D. K., & Polashenski, C. (2012). Albedo evolution of seasonal Arctic sea ice. *Geophysical Research Letters*, *39*(8). https://doi.org/10.1029/2012gl051432

Perrette, M., Yool, A., Quartly, G. D., & Popova, E. E. (2011). Near-ubiquity of ice-edge blooms in the Arctic. *Biogeosciences*, *8*(2), 515–524. https://doi.org/10.5194/bg-8-515-2011

Rainville, L., & Winsor, P. (2008). Mixing across the Arctic Ocean: Microstructure observations during the Beringia 2005 Expedition. *Geophysical Research Letters*, *35*(8), L08606. https://doi.org/10.1029/2008GL033532

Randelhoff, A., Holding, J., Janout, M., Sejr, M. K., Babin, M., Tremblay, J.-É., & Alkire, M. B. (2020). Pan-Arctic ocean primary production constrained by turbulent nitrate fluxes. *Frontiers in Marine Science*, *7*, 150. https://doi.org/10.3389/fmars.2020.00150

Redfield, A. C. (1958). The biological control of chemical factors in the environment. *American Scientist*, *46*(3), 230A–221.

Reynolds, R., Smith, T., Liu, C., Chelton, D. B., Casey, K. S., & Schlax, M. G. (2007). Daily high-resolution-blended analyses for sea surface temperature. *Journal of Climate*, *20*(22), 5473–5496. https://doi.org/10.1175/2007jcli1824.1

Sakshaug, E. (2004). *Primary and secondary production in the Arctic Seas. In The organic carbon cycle in the Arctic Ocean* (pp. 57–81). Springer. https://doi.org/10.1007/978-3-642-18912-8_3

Sakshaug, E., & Skjoldal, H. R. (1989). *Life at the ice edge*. Ambio (Sweden).

Schulze, L. M., & Pickart, R. S. (2012). Seasonal variation of upwelling in the Alaskan Beaufort Sea: Impact of sea ice cover. *Journal of Geophysical Research: Oceans*, *117*(C6). https://doi.org/10.1029/2012JC007985

Screen, J. A., & Simmonds, I. (2010). The central role of diminishing sea ice in recent Arctic temperature amplification. *Nature*, *464*, 1334–1337. https://doi.org/10.1038/nature09051

Selz, V., Saenz, B. T., Dijken, G. L., & Arrigo, K. R. (2018). Drivers of ice algal bloom variability between 1980 and 2015 in the Chukchi Sea. *Journal of Geophysical Research: Oceans*, *123*(10), 7037–7052. https://doi.org/10.1029/2018JC014123

Serreze, M. C., & Stroeve, J. (2015). Arctic sea ice trends, variability and implications for seasonal ice forecasting. *Philosophical transactions of the Royal Society of London*, *373*, 20140159. https://doi.org/10.1098/rsta.2014.0159

Sherr, B. F., Hill, V. J., Plourde, S., Stockwell, D. A., Ashjian, C. J., Sherr, E. B., & Campbell, R. G. (2008). Mesozooplankton prey preference and grazing impact in the western Arctic Ocean. *Deep Sea Research Part II: Topical Studies in Oceanography*, *56*(17), 1274–1289. https://doi.org/10.1016/j.dsr2.2008.10.027

Sherr, E. B., Sherr, B. F., & Hartz, A. J. (2009). Microzooplankton grazing impact in the Western Arctic Ocean. *Deep Sea Research Part II: Topical Studies in Oceanography*, *56*(17), 1264–1273. https://doi.org/10.1016/j.dsr2.2008.10.036

Smetacek, V. (1999). Diatoms and the ocean carbon cycle. *Protist*, *150*(1), 25–32. https://doi.org/10.1016/S1434-4610(99)70006-4

Soetaert, K., Herman, P. M. J., & Middelburg, J. J. (1996a). Dynamic response of deep-sea sediments to seasonal variations: A model. *Limnology and Oceanography*, *41*(8), 1651–1668. https://doi.org/10.4319/lo.1996.41.8.1651

Soetaert, K., Herman, P. M. J., & Middelburg, J. J. (1996b). A model of early diagenetic processes from the shelf to abyssal depths. *Geochimica et Cosmochimica Acta*, *60*(6), 1019–1040. https://doi.org/10.1016/0016-7037(96)00013-0

Soetaert, K., & Meysman, F. (2012). Reactive transport in aquatic ecosystems: Rapid model prototyping in the open source software R. *Environmental Modelling & Software*, *32*, 49–60. https://doi.org/10.1016/j.envsoft.2011.08.011

Soetaert, K., Petzoldt, T., & Setzer, R. W. (2010). Solving Differential Equations in *R* : Package deSolve. *Journal of Statistical Software*, *33*(9). https://doi.org/10.18637/jss.v033.i09

Søreide, J. E., Leu, E. V., Berge, J., Graeve, M., & Falk-Petersen, S. (2010). Timing of blooms, algal food quality and Calanus glacialis reproduction and growth in a changing Arctic. *Global Change Biology*, *16*(11), 3154. https://doi.org/10.1111/j.1365-2486.2010.02175.x

Stabeno, P. J., Mordy, C. W., & Sigler, M. F. (2020). Seasonal patterns of near-bottom chlorophyll fluorescence in the eastern Chukchi Sea: 2010–2019. *Deep Sea Research Part II: Topical Studies in Oceanography*, *177*, 104842. https://doi.org/10.1016/j.dsr2.2020.104842

Stocker, T. F., Qin, D., Plattner, G.-K., Tignor, M. M. B., Allen, S. K., Boschung, J., & Midgley, P. M. (2013). *Climate change 2013: The physical science basis* (Vol. 1535, p. 14). Cambridge university press Cambridge.

Strass, V. H., & Nöthig, E. M. (1996). Seasonal shifts in ice edge phytoplankton blooms in the Barents Sea related to the water column stability. *Polar Biology*, *16*(6), 409–422. https://doi.org/10.1007/BF02390423

Stroeve, J., Liston, G. E., Buzzard, S., Zhou, L., Mallett, R., Barrett, A., et al. (2020). A Lagrangian snow evolution system for sea ice applications (SnowModel-LG): Part II—analyses. *Journal of Geophysical Research: Oceans*, *125*(10). https://doi.org/10.1029/2019JC015900

Teal, L., Bulling, M., Parker, E., & Solan, M. (2008). Global patterns of bioturbation intensity and mixed depth of marine soft sediments. *Aquatic Biology*, *2*(3), 207–218. https://doi.org/10.3354/ab00052

Tschudi, M., Meier, W. N., Stewart, J. S., Fowler, C., & Maslanik, J. (2019). *EASE-grid sea ice age, version 4. NASA national snow and ice data center DAAC*.

Tschudi, M., Stroeve, J., & Stewart, J. (2016). Relating the age of Arctic Sea Ice to its Thickness, as measured during NASA's ICESat and IceBridge campaigns. *Remote Sensing*, *8*(6), 457. https://doi.org/10.3390/rs8060457

Webster, M. A., Rigor, I. G., Perovich, D. K., Richter-Menge, J. A., Polashenski, C. M., & Light, B. (2015). Seasonal evolution of melt ponds on Arctic sea ice. *Journal of Geophysical Research: Oceans*, *120*(9), 5968–5982. https://doi.org/10.1002/2015JC011030

Welch, H. E., & Bergmann, M. A. (1989). Seasonal development of ice algae and its prediction from environmental factors near resolute, N.W.T., Canada. *Canadian Journal of Fisheries and Aquatic Sciences*, *46*(10), 1793–1804. https://doi.org/10.1139/f89-227

Woodgate, R. A., Aagaard, K., & Weingartner, T. J. (2005). A year in the physical oceanography of the Chukchi Sea: Moored measurements from autumn 1990–1991. *Deep Sea Research Part II: Topical Studies in Oceanography*, *52*(24–26), 3116–3149. https://doi.org/10.1016/j.dsr2.2005.10.016

Woodgate, R. A., Weingartner, T. J., & Lindsay, R. (2012). Observed increases in Bering Strait oceanic fluxes from the Pacific to the Arctic from 2001 to 2011 and their impacts on the Arctic Ocean water column. *Geophysical Research Letters*, *39*(24), 2012GL054092. https://doi.org/10.1029/2012GL054092

Yager, P. L., Connelly, T. L., Mortazavi, B., Wommack, K. E., Bano, N., Bauer, J. E., et al. (2001). Dynamic bacterial and viral response to an algal bloom at subzero temperatures. *Limnology and Oceanography*, *46*(4), 790–801. https://doi.org/10.4319/lo.2001.46.4.0790

Zhou, L., Stroeve, J., Xu, S., Petty, A., Tilling, R., Winstrup, M., et al. (2021). Inter-comparison of snow depth over Arctic sea ice from reanalysis reconstructions and satellite retrieval. *The Cryosphere*, *15*(1), 345–367. https://doi.org/10.5194/tc-15-345-2021